23. CHEMICAL PROFILES IN SEDIMENT AND BASALT SAMPLES FROM DEEP SEA DRILLING PROJECT LEG 74, HOLE 525A, WALVIS RIDGE[1]

Yun-Gang Liu[2] and Roman A. Schmitt, Department of Chemistry and the Radiation Center, Oregon State University, Corvallis, Oregon

ABSTRACT

Forty sediment and four basement basalt samples from DSDP Hole 525A, Leg 74, as well as nine basalt samples from southern and offshore Brazil, were subjected to instrumental neutron activation analysis. Thirty-two major, minor, and trace elements were determined.

The downcore element concentration profiles and regression analyses show that the rare earth elements (REE) are present in significant amounts in both the carbonate and noncarbonate phases in sediments; Sr is concentrated in the carbonate phase, and most of the other elements determined exist mainly in the noncarbonate phase.

The calculated partition coefficients of the REE between the carbonate phase and the free ion concentrations in seawater are high and increase with decreasing REE ionic radii from 3.9×10^6 for La to 15×10^6 for Lu. Calculations show that the lanthanide concentrations in South Atlantic seawater have not been changed significantly over the past 70 Ma.

The Ce anomaly observed in the carbonate phase is a redox indicator of ancient seawater. Study of the Ce anomaly reveals that seawater was anoxic over the Walvis Ridge during the late Campanian. As the gap between South America and West Africa widened and the Walvis Ridge subsided from late Campanian to late Paleocene times, the water circulation of the South Atlantic improved and achieved oxidation conditions about 54 Ma that are similar to present seawater redox conditions in the world oceans.

The chemical compositions of the basement rocks correspond to alkalic basalts, not mid-ocean ridge basalts (MORBs). The results add more evidence to support the hypothesis that the Walvis Ridge was formed by a series of volcanos moving over a "hot spot" near the Mid-Atlantic Ridge.

From the chemical composition and REE pattern, one 112 Ma old basalt on the Brazilian continental shelf has been identified as an early stage MORB. To date, this is the oldest oceanic tholeiite recovered from the South Atlantic. This direct evidence indicates that the continental split between South America and Africa commenced ≥ 112 Ma.

INTRODUCTION

The Walvis Ridge, like the São Paulo Plateau–Rio Grande Rise Complex, presents a major barrier to South Atlantic water circulation. The pronounced effects from restricted circulation would be expected to be aggravated by narrower separations of the South American and African continents. Also, it has been suggested that the Walvis Ridge represents a chain of volcanoes which drifted continuously over a hot spot near the Mid-Atlantic Ridge as the two continents were moving apart, consistent with the theory of seafloor spreading (Wilson, 1963, 1965). In these and other respects, then, the study of Walvis Ridge will enhance our understanding of South Atlantic oceanic history.

Larson and Ladd (1973) have determined from the marine magnetic anomalies in the southern South Atlantic that the initial rift of the South American and African continents occurred in the Early Cretaceous, probably in the Valanginian (~125 to 130 Ma). The early opening of the southern South Atlantic continued up to at least 112 Ma. According to paleontological studies (Reyment, 1969), subsequent rifting may have been completed by the Aptian (~110 Ma) or earlier. To the north, west central Africa and northeast Brazil were finally separated during the late early Turonian (~90 Ma), thereby uniting the North and South Atlantic oceans.

Sites previously drilled on the Walvis Ridge are Sites 362 and 363, Leg 40, on the Frio Ridge close to Africa, and Site 359, Leg 39, at the seamounts near the Mid-Atlantic Ridge.

In this paper, we present the results of the analysis of major, minor, and trace elements in sediment and basement rock samples obtained from a 678 m hole drilled by the DSDP at Hole 525A, Leg 74 (June 10–15, 1980), on the Walvis Ridge. The rare earth element (REE) distributions will be emphasized in our discussions. Interpretation of the varying patterns of the REE abundances has become an important tool in geochemistry (e.g., Haskin et al., 1966, and Haskin and Paster, 1979). The REE as a group are relatively coherent because, under most natural conditions, all lanthanides exist in a common trivalent state. Abundance anomalies occur under some special redox conditions for Ce (+3 and +4) and Eu (+2 and +3). Therefore, observed anomalies of Ce or Eu are indicators of redox environments.

The REE concentrations and the relative abundances of individual REE are different for different geological materials. This makes it possible to use REE concentrations and their distribution patterns to identify the different constituent materials and to understand their genesis. Haskin et al. (1966) and Haskin and Paster (1979) have summarized REE geochemistry in meteorites and in sedimentary and igneous rocks. Use of the REE as a geochemical tool began in the early 1960s with the de-

[1] Moore, T. C., Jr., Rabinowitz, P. D., et al., *Init. Repts. DSDP*, 74: Washington (U.S. Govt. Printing Office).

[2] Present address: Institute of Atomic Energy, Academy of Sciences P.O. Box 275(58), Beijing, China.

Table 1. Element concentrations of sediment samples, Hole 525A.

Element	Core-Section (interval in cm) 1-3, 15-17 (3.2)[a]	4-1, 35-36 (51.5)	6-2, 80-82 (100.9)	7-5, 41-42 (171.5)	10-7, 40-41 (203.0)	13-7, 20-21 (230.3)	17-1, 10-11 (260.2)	22-1, 45-46 (298.6)	25-1, 23-24 (326.8)	26-1, 3-4 (336.1)	26-1, 62-63 (336.7)	26-2, 84-85 (338.4)	26-2, 84-85 (338.4)	27-1, 35-36 (345.9)	28-2, 10-11 (353.2)	29-4, 10-11 (359.7)
Major Elements (%)																
Ti	0.02	0.02	0.01	0.03	0.05	0.02	0.02	0.01	0.03	0.02	0.02	0.02	—	0.02	0.01	0.03
Al	0.21	0.22	0.15	0.35	0.53	0.20	0.47	0.11	0.28	0.26	0.16	0.27	—	0.18	0.15	0.23
Fe	0.15	0.14	0.10	0.22	0.35	0.12	0.26	0.07	0.12	0.16	0.13	0.17	0.18	0.12	0.09	0.12
Mg	0.3	0.2	0.1	0.2	0.2	0.2	0.3	0.2	0.2	0.2	0.3	0.2	—	0.2	0.2	0.2
Ca	39.4	39.2	39.8	38.9	37.7	39.3	37.8	39.0	39.2	39.6	38.4	38.4	—	38.4	38.7	38.4
Na	0.66	0.48	0.53	0.50	0.49	0.48	0.46	0.65	0.70	0.56	0.59	0.56	0.57	0.72	0.41	0.48
K	0.07	0.04	0.08	0.11	0.16	0.07	0.19	0.04	0.15	0.06	0.07	0.11	0.12	0.10	0.09	0.12
Cl	1.15	0.78	0.93	0.87	0.77	0.84	0.70	1.20	1.14	0.90	0.97	0.94	—	1.18	0.68	0.75
Minor and Trace Elements (ppm)																
Br	28	20	24	23	21	23	20	31	33	25	29	25	31	31	21	22
Sc	0.93	0.84	0.67	1.27	1.94	0.81	1.37	0.54	0.94	0.90	1.07	1.05	1.05	0.80	0.85	0.86
V	3.9	2.6	2.5	5.1	9.6	2.9	7.0	1.3	4.2	4.9	2.7	4.8	—	2.6	1.5	2.6
Cr	2.6	2.3	1.9	2.6	3.6	1.2	2.6	1.3	3.1	3.3	2.2	2.9	3.1	5.4	1.4	1.4
Mn	166	185	112	227	370	158	200	109	219	196	329	184	—	197	152	288
Co	2.8	1.8	2.3	3.2	6.3	3.6	2.6	0.83	1.96	3.0	1.64	2.1	2.3	1.92	0.80	1.52
Zn	3.0	3.1	2.1	2.6	3.8	2.7	5.2	1.2	2.1	2.2	4.6	2.4	2.9	2.3	2.2	3.1
As	0.3	0.2	0.7	0.4	0.5	0.2	0.3	0.02	0.10	0.04	0.10	0.06	0.02	0.05	0.15	0.19
Rb	2.7	3.6	3.1	4.9	8.7	3.5	8.3	2.2	3.9	4.1	2.7	5.3	5.2	2.8	2.0	2.7
Sr	1280	1270	1220	1350	1190	1250	1090	1250	1080	1170	550	1080	1210	1210	670	720
Ba	290	330	110	120	60	270	310	170	180	170	760	160	160	140	570	680
La	4.9	5.4	4.7	7.3	8.9	5.4	8.4	4.5	5.8	6.1	9.4	5.9	5.8	5.3	8.9	7.2
Ce	4.3	4.6	3.2	5.6	8.7	4.1	6.9	2.4	5.5	4.6	6.8	4.9	5.1	3.8	6.6	6.0
Nd	5.0	6.2	4.9	8.0	8.8	5.9	8.9	4.3	6.2	6.3	10	6.1	5.6	5.1	10.3	8.5
Sm	0.86	1.06	0.94	1.50	1.93	1.08	1.58	0.79	1.25	1.25	1.74	1.24	1.24	1.08	1.65	1.31
Eu	0.22	0.25	0.21	0.33	0.43	0.24	0.34	0.17	0.30	0.27	0.38	0.27	0.27	0.25	0.42	0.31
Tb	0.16	0.15	0.14	0.21	0.28	0.14	0.24	0.11	0.19	0.20	0.26	0.16	0.19	0.17	0.29	0.22
Dy	1.1	1.2	0.96	1.3	1.7	0.96	1.5	0.80	1.5	1.4	1.7	1.2	—	1.1	1.6	1.4
Yb	0.71	0.65	0.44	0.77	0.91	0.54	0.85	0.46	0.70	0.61	0.92	0.60	0.64	0.54	0.92	0.71
Lu	0.11	0.10	0.061	0.11	0.12	0.082	0.12	0.057	0.095	0.083	0.14	0.088	0.086	0.072	0.012	0.092
Hf	0.09	0.08	0.06	0.15	0.26	0.10	0.25	0.05	0.08	0.11	0.09	0.11	0.11	0.08	0.08	0.11
Ta	0.024	0.029	0.026	0.055	0.076	0.020	0.061	0.022	0.037	0.027	0.020	0.027	0.016	0.027	0.048	0.029
Th	0.10	0.16	0.11	0.32	0.50	0.23	0.54	0.18	0.52	0.52	0.31	0.53	0.59	0.37	0.33	0.36
U	—	—	—	—	—	—	—	—	—	—	—	—	—	—	—	—
Noncarbonate (%)	2	2	0.5	3	6	2	6	3	2	1	4	4	(4)	4	3	4

Note: The average counting errors are <5% for Al, Fe, Ca, Na, Cl, Sc, Cr, Mn, Co, La, and Sm; 5-10% for V, Ce, Eu, Tb, Yb, Lu, Hf, Ta, and Th; 10-20% for Ti, Mg, K, Br, As, Rb, Sr, Ba, and Dy; 20-30% for Zn, Nd, and U. A dash indicates that the element was not detected.

[a] Sub-bottom depth, in meters, in parentheses.

velopment of accurate neutron activation techniques for their analysis. The neutron activation analysis techniques and their applications to geological materials have been discussed recently by Laul (1979).

EXPERIMENTAL

Sample Preparation

The water-containing DSDP samples were broken in an agate mortar, then dried in a freeze-drier for 24 hr. Samples were weighed and dried another 24 hr. and then weighed again. The two weights were consistent. All dried samples contained the salt which was originally present in the interstitial water. All sample weights were corrected for their salt content by subtracting the salt weight contained in the interstitial water. Also, the element concentrations were corrected by subtracting the contribution from interstitial water. This will be discussed later.

A mollusk shell fragment sample (*Inoceramus.*) was analyzed. The mollusk sample, which was picked from Upper Cretaceous sediments in Cores 525A-50-52 was obtained from Anne Boersma, Lamont-Doherty Geological Observatory, Columbia University. The shell fragments were cleaned with ethanol in an ultrasonic cleaner for 30 min. to remove an adhering oxide matter. Microscopic examination revealed clean fragment surfaces. The dried DSDP sediment samples and the pulverized and powdered basalt samples, ~500 mg, and a mollusk sample, ~40 mg, were weighed into polyethylene vials and heat-sealed for neutron activation analysis.

Activation and Counting

A standard sequential instrumental neutron activation analysis (INAA) procedure (Laul, 1979) was used. Activations were done in the 1 MW TRIGA reactor at the Radiation Center of Oregon State University. The counting system consisted of a Ge(Li) detector coupled with an ND600 analyzer (4096 channels). All data were computer-reduced.

Sediment samples from 47 core locations and 1 mollusk sample were analyzed as two groups. Analysis of the first group of 40 samples (39 sediment and 1 mollusk sample) consisted of both short and long activations (Laul, 1979), followed by a count of the short and long-lived radionuclides, respectively. A significant change in the La/Ce ratio (Ce depletion) was observed for the first batch of samples from Cores 525A-26 and 525A-31. Because these data were essential for the interpretation of changes in the anoxic conditions in seawater over the Walvis Ridge, another batch of 11 samples (525A-25-1, 23-24 cm; 525A-26-1, 3-4 cm; 525A-26-1, 62-63 cm; 525A-26-2, 84-85 cm; 525A-27-1, 35-36 cm; 525A-28-2, 10-11 cm; 525A-29-4, 10-11 cm; 525A-30-4, 50-51 cm; 525A-31-3, 5-6 cm; 525A-35-4, 130-131 cm; 525A-36-3, 15-16 cm) was subjected to short and long activations primarily for their REE pattern characterization. In this latter group of 11 samples, three samples (525A-26-2, 84-85 cm; 525A-31-3, 5-6 cm; 525A-35-4, 130-131 cm) were aliquants of previously analyzed sample powders. The results of Hole 525A sediment samples are presented in Table 1. The results of Hole 525A basement rock and other basalt samples are tabulated in Table 2.

As previously mentioned, the DSDP sediment contained interstitial water. When samples were dried, the salts originally in the interstitial water remained within the samples. From the measured quantities of interstitial water in the total sample, the element concentrations in the dried sediment samples minus the seawater contributions were estimated. Since the variations in interstitial seawater are probably not too large, we used the average composition of seawater for estimating the contributions of interstitial water. Calculations using average seawater compositional data (Turekian, 1968) and the measured water contents in our sediment samples indicate that almost all the Cl and Br contents in our sediment samples may be attributed to interstitial water. The contributions of Mg, Na, and K from interstitial water are also significant. Since the concentrations of Ca in Walvis Ridge calcareous sediments are high, the interstitial water contributions to Ca are relatively insignificant. For all other elements analyzed in this work, the concentrations in seawater are much lower than in sediments and therefore the interstitial-water contribution may be ignored.

Table 1. (Continued).

Core-Section (interval in cm)																		
30-4, 50-51 (369.6)	31-3, 5-6 (377.2)	31-3, 5-6 (377.2)	35-4, 130-131 (408.4)	35-4, 130-131 (408.4)	36-3, 15-16 (415.3)	38-3, 119-120 (435.3)	42-1, 50-51 (469.6)	44-4, 50-52 (493.1)	45-4, 53-54 (502.6)	46-3, 22-23 (510.3)	47-4, 30-31 (521.4)	48-1, 105-106 (527.2)	50-1, 70-71 (545.8)	50-2, 70-71 (547.3)	50-3, 124-126 (549.4)	50-4, 70-71 (550.3)	50-5, 70-71 (551.8)	50-6, 80-81 (553.4)
0.02	0.03	0.02	0.04	0.05	0.03	0.08	0.17	0.54	0.23	0.45	0.81	0.38	0.33	0.27	0.26	0.29	0.28	0.43
0.25	0.29	0.29	0.75	0.78	0.41	0.99	2.45	5.23	3.00	4.33	4.55	2.74	3.41	2.80	3.01	2.89	3.12	2.93
0.13	0.22	0.22	0.39	0.38	0.19	0.68	1.64	4.02	2.50	2.98	5.11	2.51	2.76	1.99	2.14	2.15	2.62	2.58
0.2	0.2	0.2	0.4	0.3	0.1	0.3	0.8	1.9	0.9	1.5	1.8	0.8	1.3	0.8	0.7	0.9	1.0	1.1
39.7	38.4	38.5	35.1	34.7	37.8	34.1	27.8	10.6	23.2	17.3	12.1	18.8	17.3	25.1	14.1	24.5	20.8	24.5
0.44	0.45	0.54	0.47	0.46	0.49	0.54	0.55	1.23	0.91	1.47	1.20	0.72	0.75	0.74	0.64	0.85	0.78	0.78
0.13	0.13	0.17	0.26	0.39	0.22	0.43	0.80	1.7	0.86	1.45	1.60	0.96	1.24	0.97	1.03	1.03	1.17	1.33
0.71	0.74	0.82	0.63	0.58	0.68	0.57	0.25	0.60	0.44	0.56	0.47	0.36	0.43	0.36	0.32	0.40	0.34	0.34
20	20	23	17.4	21	22	15.1	7.2	11.7	11.4	10.9	9.8	10.0	11.8	10.6	8.7	11.6	11.0	19.0
0.87	1.27	1.27	1.80	1.77	1.01	2.7	4.5	13.3	4.9	7.8	17.6	7.5	8.7	9.3	6.99	8.67	9.41	8.44
2.1	3.1	2.7	8.7	8.3	5.2	16	32	114	33	64	168	62	78	71	59	60	74	65
1.9	2.0	2.2	3.9	4.4	1.9	7.6	12	40	12	19	22	16	32	26	21	40	32	47
138	87	100	249	268	292	299	550	490	1090	816	536	665	497	781	356	891	658	960
1.02	2.9	2.9	3.3	3.3	1.62	2.6	4.6	22.7	5.3	7.3	37	7.7	7.4	22.0	10.1	29.5	9.8	9.7
4.0	6.5	5.7	6.8	6.6	10.3	23	41	92	37	96	65	43	48	60	50	52	73	43
0.25	0.5	0.17	0.16	0.09	0.06	0.4	0.8	2.0	0.7	1.0	2.7	0.6	2.1	4.5	1.1	3.6	1.6	0.9
3.7	5.8	4.6	14	13.2	5.7	10	26	74	28	41	59	42	48	34	42	32	43	48
740	780	860	920	970	990	830	720	580	820	710	440	500	510	810	510	710	630	520
630	690	680	890	830	520	200	330	570	320	380	550	640	910	930	760	1040	1380	1240
6.4	9.8	9.9	11.6	11.8	7.4	13.8	23.5	27.1	35.6	49.3	17.9	16.3	16.0	19.5	14.1	19.0	17.2	16.4
5.1	12.5	12.6	14.5	14.0	9.4	19.8	46	63	71	104	39	29	31	34	29	35	32	33
6.9	10	11.7	11	12.5	8.6	14	18	25	28	46	20	13	14	18	11	19	12	11
1.13	1.87	1.87	1.97	1.97	1.25	2.39	4.15	4.80	6.49	8.17	3.80	3.00	2.85	3.85	2.56	3.63	3.29	2.99
0.28	0.49	0.52	0.40	0.38	0.26	0.48	0.59	1.2	0.83	0.98	1.0	0.67	0.66	0.87	0.61	0.87	0.81	0.79
0.19	0.32	0.37	0.29	0.42	0.18	0.37	0.62	0.72	0.94	1.4	0.70	0.39	0.34	0.56	0.35	0.52	0.48	0.41
1.4	2.0	1.9	1.8	2.0	1.2	2.5	3.7	4.3	6.0	7.7	3.9	2.3	2.6	3.4	2.3	3.1	3.0	3.3
0.62	0.99	0.95	1.0	1.04	0.61	1.2	2.2	2.4	3.6	5.6	2.1	1.5	1.4	1.9	1.1	1.7	1.7	1.3
0.086	0.13	0.13	0.14	0.16	0.090	0.16	0.29	0.37	0.50	0.80	0.31	0.19	0.19	0.28	0.17	0.26	0.24	0.20
0.15	0.23	0.18	0.77	0.80	0.36	1.1	3.9	4.1	8.1	8.9	3.7	2.0	2.2	2.2	1.9	1.7	2.3	1.7
0.038	0.090	0.090	0.28	0.27	0.16	0.45	1.3	1.7	2.5	3.3	1.1	0.57	0.65	0.62	0.52	0.56	0.62	0.60
0.36	1.1	0.60	5.2	1.4	0.70	1.5	4.9	7.4	7.4	9.4	4.0	3.7	4.4	3.1	3.9	2.7	3.4	2.7
—	—	—	—	0.5	—	0.4	1.0	2.2	1.5	2.8	1.1	0.9	1.0	1.1	0.9	1.0	1.1	0.3
1	4	4	13	13	5	16	36	79	45	61	75	57	61	40	70	42	52	42

DISCUSSION

The Downcore Element Concentration Profiles

Marine sediments are composed mainly of calcium carbonate, opal, and noncarbonate phases (clay, sand, or sandstone, etc.); in our samples, most noncarbonate phases are clay. If it is assumed that the sediments consist of only two components, carbonate and clay, the carbonate and noncarbonate fractions in all samples can be simply calculated, because the Ca concentrations in the samples and in average clay (2.9% Ca; Turekian and Wedepohl, 1961) are known. Since only a few samples contain mineral clay detritus and only a small fraction of Ca is present in the clay or sandstone, the error introduced by this assumption is insignificant.

It is likely that many important geologic events occurred during the formation of the earlier sediments (Hole 525A) on the Walvis Ridge. Over time, the bottom sediments were indurated to increasing degrees. Therefore, more samples close to the basalt/sediment interface were analyzed relative to the monotonous and predominantly $CaCO_3$ phase (>95%) in the top ~400 m of the sedimentary core. For the same reason, we plotted the downcore element concentration profiles in logarithmic units for the stratigraphic distance above the basalt/sediment interface to emphasize the lower and compacted part of the Hole 525A core.

Figure 1 shows the downcore variation profiles of noncarbonate and some representative elements: Al, La, and Sr. Downcore profiles of other elements, Ti, Fe, Mg, Na, K, Cl, Br, Sc, V, Cr, Mn, Co, Zn, As, Rb, Ba, Ce, Nd, Sm, Eu, Tb, Dy, Yb, Lu, Hf, Ta, and Th, are presented by Liu (1982). Two interesting features are apparent from these diagrams:

1) Though the short-term trends appear complex, the noncarbonate content decreased rapidly over the long term, starting with Section 525A-44-4 (~79% noncarbonate, mid-Maestrichtian, ~68 Ma). This probably reflects decreasing contributions of solid sedimentary material from the African continent and/or a decrease in weathered products from a Walvis Ridge subsiding to below sea level, in conjunction with decreasing volcanic activity on the nearby Walvis Ridge itself. Beginning with Section 525A-31-3 (377 m sub-bottom, late Paleocene, ~54 Ma), the noncarbonate content became quite low (≤5%) and not much change is noted in the composition of the overlying sedimentary column, indicating a relatively stable state of carbonate deposition during the past ~54 Ma. The data for Section 525A-36-3 strongly indicate a 5% noncarbonate component; that for Section 525A-35-4 has a ~13% noncarbonate content.

2) There are some congruent relationships between certain diagnostic element abundances and the noncarbonate content. As expected, the profile of Al (Fig. 1B) follows the noncarbonate content very well, indicating that Al is associated with the noncarbonate (primarily aluminosilicate) component in sediments. La (Fig. 1C), as a representative incompatible REE, basically follows the noncarbonate content. However, in Samples 525A-45-4, 53–54 cm and 525A-46-3, 22–23 cm, the La concentrations are much higher than in other samples. These samples will be discussed later. The profile of Sr is shown in Fig. 1D. As expected, Sr substitutes for Ca in the carbonate component. Profiles of most of the

Table 1. (Continued).

Element	Core-Section (interval in cm) 50-7, 12-13 (554.2)	51-1, 79-80 (555.4)	51-2, 60-61 (556.7)	51-3, 40-41 (558.0)	51-4, 80-81 (559.9)	51-5, 145-147 (562.1)	51-6, 70-71 (562.8)	52-1, 50-51 (564.6)	52-2, 50-51 (566.1)	52-3, 100-101 (568.1)	52-4, 50-51 (569.1)	52-5, 11-12 (570.2)	53-1, 19-20 (573.8)	53-1, 53-54 (574.1)	53-1, 75-76 (574.4)	Mollusk
Major Elements (%)																
Ti	0.23	0.30	0.70	0.70	0.52	0.35	0.26	0.50	0.46	0.45	0.35	0.48	0.47	0.45	0.60	—
Al	2.42	2.49	4.32	5.09	3.65	3.20	2.66	3.21	3.12	2.87	2.60	5.44	2.82	4.58	4.97	0.03
Fe	1.87	2.56	3.36	6.08	3.94	2.89	3.11	2.42	2.52	3.05	4.25	6.38	8.51	3.07	11.8	0.33
Mg	0.6	0.8	1.5	1.6	1.4	1.0	0.8	0.9	0.9	1.5	1.3	2.0	1.4	1.5	2.5	—
Ca	22.9	25.3	18.6	12.8	20.1	21.1	24.7	23.0	24.2	23.7	24.0	10.3	18.1	18.0	1.10	40.0
Na	0.64	0.66	1.33	1.36	0.89	0.70	0.64	0.97	1.10	0.84	0.72	1.51	0.64	1.47	0.92	0.18
K	0.89	0.90	1.55	2.02	1.43	1.23	1.34	0.98	1.05	1.08	1.31	1.02	1.45	1.61	2.68	—
Cl	0.41	0.31	0.34	0.37	0.39	0.32	0.31	0.33	0.28	0.28	0.33	0.50	0.28	0.21	0.34	—
Minor and Trace Elements (ppm)																
Br	25.0	19.6	20.1	21.7	22.8	17.5	19.7	23.0	17.9	22.0	20.0	26.3	16.6	13.0	21.8	2.1
Sc	6.21	7.05	12.1	14.6	10.7	8.35	7.40	7.99	8.55	8.50	7.23	16.8	11.0	10.3	17.6	2.92
V	58	55	110	123	80	70	58	70	75	85	72	193	152	98	214	—
Cr	17	22	22	34	36	22	20	23	27	23	22	50	31	38	50	2.5
Mn	756	1100	780	816	831	834	1120	773	799	903	1300	1150	1760	1720	903	2110
Co	8.6	6.2	10.5	14.7	12.0	7.6	8.9	9.7	6.1	6.9	8.2	7.7	13.3	220	47	4.7
Zn	50	49	50	89	78	50	47	30	32	34	40	123	110	63	140	10
As	0.4	0.9	1.4	1.2	1.2	1.6	2.9	2.1	1.4	1.9	1.6	0.2	14	6.5	18	0.9
Rb	40	38	44	71	64	60	51	31	27	40	53	26	49	36	111	—
Sr	380	430	440	360	450	360	390	460	520	430	470	540	650	820	40	830
Ba	850	600	570	610	720	570	390	280	230	270	410	200	570	320	1130	40
La	16.5	18.0	25.7	24.4	20.9	20.2	18.6	17.4	16.0	21.8	21.9	28.5	20.3	27.2	26.2	10.6
Ce	28	33	47	53	42	40	38	31	32	39	38	58	34	55	49	17
Nd	12	13	18	24	17	18	15	14	10	13	13	21	9	15	23	7
Sm	2.71	3.25	3.94	4.18	3.63	3.49	3.37	2.73	2.54	3.56	3.34	5.43	3.33	4.09	5.38	1.27
Eu	0.64	0.72	1.1	1.2	0.92	0.79	0.76	0.71	0.73	0.79	0.77	1.2	0.84	1.2	1.2	0.34
Tb	0.34	0.43	0.54	0.59	0.48	0.46	0.44	0.35	0.37	0.46	0.48	0.65	0.52	0.65	0.74	0.20
Dy	2.0	2.5	3.6	3.7	2.7	2.8	2.9	2.2	2.4	2.5	3.0	3.7	2.7	4.2	3.8	1.4
Yb	1.4	1.8	1.6	1.9	1.7	1.6	1.5	1.3	1.0	1.7	1.7	2.2	2.0	2.2	2.8	1.3
Lu	0.20	0.25	0.24	0.24	0.26	0.23	0.22	0.17	0.15	0.24	0.26	0.37	0.30	0.34	0.43	0.19
Hf	1.5	1.8	2.5	2.9	2.4	2.2	1.8	2.0	1.9	2.8	2.0	4.2	2.3	3.1	4.2	—
Ta	0.53	0.51	1.1	1.2	0.88	0.69	0.60	0.77	0.77	0.86	0.64	1.3	0.62	1.2	1.1	—
Th	2.6	2.5	4.0	4.8	4.5	4.1	3.6	2.5	2.2	3.1	3.0	7.8	2.5	4.0	6.0	0.10
U	0.5	0.4	0.4	0.6	0.8	1.2	1.8	1.9	0.7	1.1	1.0	4.7	1.1	0.8	1.1	0.7
Noncarbonate (%)	46	40	58	73	54	51	41	46	43	44	43	80	59	59	100	

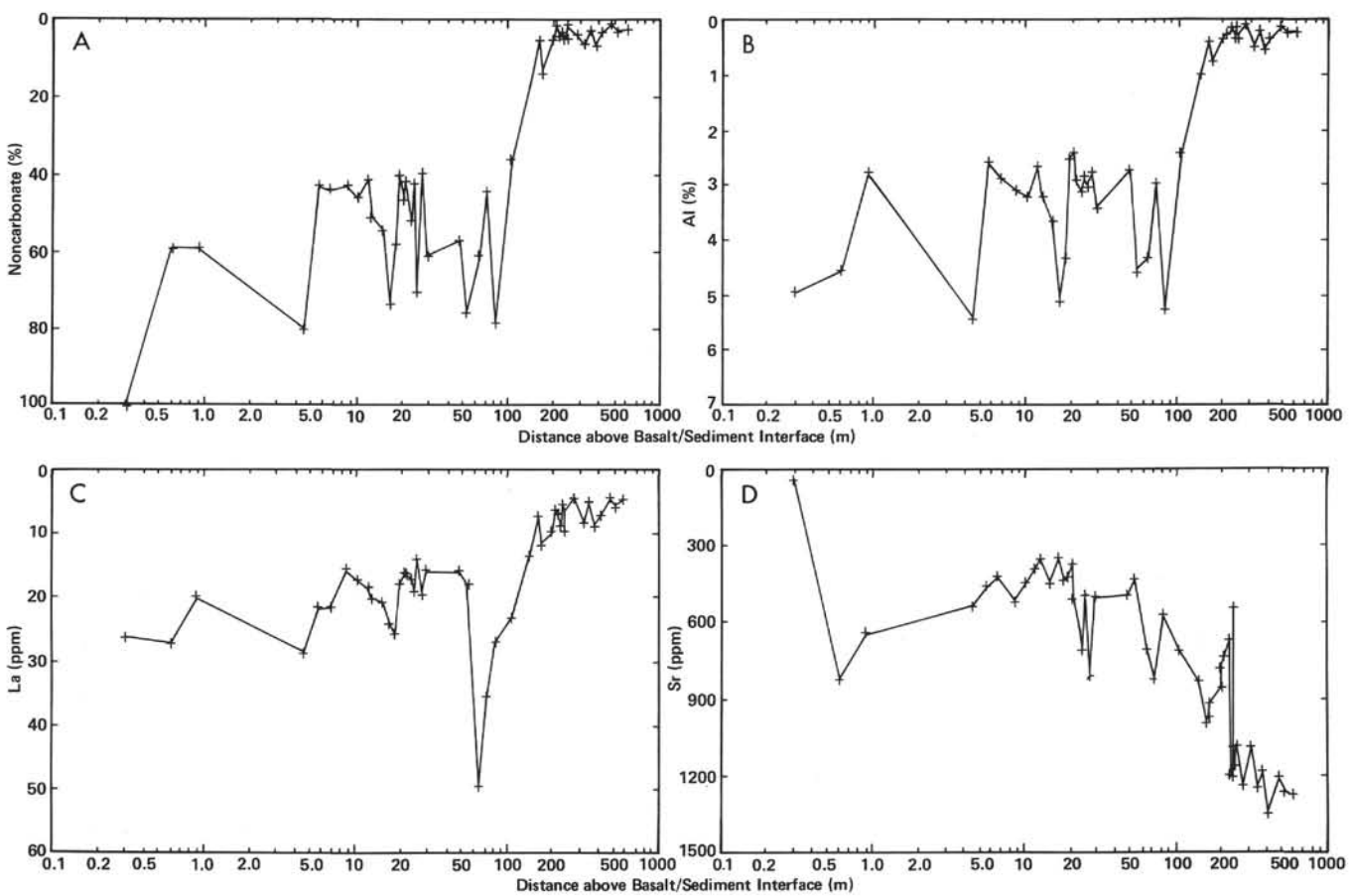

Figure 1. Downcore element concentration profiles in Hole 525A. A. Noncarbonate material. B. Al. C. La. D. Sr.

Table 2. Element concentrations of basalt samples.

Element	Hole 525A[a] (piece no. in parens)				Parana, S. Brazil[b]		Espírito Santo[c]		Southeastern Margin, Brazil[c]				
	53-1(1D)	53-3(7A)	58-2(2H)	63-1(2A)	PAR-1	PAR-2	IP-1-ES	NIES 1/1	SPS-4A	RJS-33	RJS-36	RJS-87	ESS-9
Major elements (%)													
TiO_2	3.08	2.63	3.05	3.22	3.62	1.52	0.92	2.69	1.48	1.40	1.17	1.33	2.59
Al_2O_3	19.6	18.2	16.0	15.6	13.5	12.8	13.4	11.3	13.7	12.8	12.7	12.7	14.0
FeO	3.38	5.52	8.25	9.10	12.6	12.4	10.6	15.9	11.5	10.8	12.1	11.4	8.98
MgO	2.4	2.4	2.5	4.3	5.1	5.1	7.5	5.6	5.8	11.1	7.3	8.0	5.5
CaO	7.6	8.1	9.4	7.8	9.0	8.5	12.2	8.7	9.1	8.5	10.6	8.0	10.1
Na_2O	4.08	3.93	3.75	3.91	2.82	2.71	2.11	2.40	1.59	2.36	3.19	3.32	2.74
K_2O	1.0	1.0	1.1	1.9	1.8	1.0	0.2	1.2	0.8	0.8	0.4	0.9	1.0
MnO	0.006	0.050	0.079	0.123	0.160	0.197	0.285	0.274	0.149	0.166	0.215	0.265	0.117
Minor and trace elements (ppm)													
Sc	37	39	39	29	26	34	49	45	38	26	52	49	24
V	453	420	410	340	340	400	310	760	370	210	380	340	250
Cr	315	301	48	39	96	16	82	52	47	433	72	174	222
Co	100	54	37	44	79	157	50	67	45	79	55	50	41
Ni	50	50	30	70	70	—	40	40	40	290	40	60	80
Zn	90	63	140	121	110	110	133	147	70	100	159	138	80
Rb	6	13	4	15	37	35	8	29	15	18	16	7	21
Cs	—	—	—	—	0.4	0.9	—	—	0.3	—	1.9	—	—
Sr	480	470	570	460	670	150	80	—	310	—	150	250	460
Ba	280	280	420	540	550	440	100	470	220	180	110	290	310
La	23.2	20.7	29.2	42.2	34.1	25.4	7.1	32.0	13.7	8.2	4.7	12.0	30.7
Ce	53	47	68	89	78	54	15	74	32	22	14	29	69
Nd	29	21	27	46	42	25	9	44	19	12	10	19	34
Sm	7.30	6.07	7.71	9.5	9.08	5.43	2.66	8.07	4.66	3.32	3.39	4.53	7.39
Eu	2.3	2.0	2.3	3.1	3.1	1.7	0.87	2.2	1.7	1.2	1.2	1.4	2.3
Tb	1.09	0.95	1.01	1.35	1.23	0.85	0.57	1.29	0.85	0.63	0.76	0.85	0.91
Dy	6.0	4.7	7.1	7.7	7.7	5.4	4.7	7.9	5.0	3.7	5.3	6.1	4.9
Yb	2.7	2.9	2.9	3.2	2.5	3.1	3.1	4.5	2.8	1.7	3.4	3.4	1.9
Lu	0.34	0.41	0.42	0.51	0.41	0.48	0.47	0.76	0.44	0.25	0.55	0.54	0.31
Zr	150	110	160	190	220	130	—	240	150	—	100	110	220
Hf	5.2	5.0	6.1	8.6	7.4	4.3	1.9	5.5	3.2	2.3	2.3	3.2	5.1
Ta	1.13	0.92	1.52	2.06	1.94	1.8	0.9	2.5	0.6	1.4	0.6	0.8	2.8
Th	2.9	2.2	3.0	5.4	3.8	4.5	2.5	3.7	1.4	1.0	0.32	1.1	3.1
U	0.7	0.6	0.7	1.4	1.1	1.2	0.6	0.8	—	—	—	—	0.8

Note: The average counting errors are: <5% for Al, Fe, Na, Mn, Sc, V, Cr, Co, La, and Sm; 5-10% for Mg, Ca, Ce, Eu, Tb, Yb, Lu, Hf, Ta, and Th; 10-20% for Ti, Rb, Sr, Ba, and Dy; 20-30% for K, Ni, Zn, Cs, Nd, Zr, and U. A dash indicates that the element was not detected.

[a] The distances below the basalt/sediment interface for 525A-53-1(1D), 525A-53-3(7A), 525A-58-2(2H), and 525A-63-1(2A) are 0.24, 2.8, 48.7, and 94.12 m, respectively.

[b] These samples were obtained from G. J. Wasserburg, Division of Geological and Planetary Sciences, California Institute of Technology.

[c] These samples, all from Brazil, were obtained from R. V. Fodor, Department of Marine, Earth, and Atmospheric Sciences, North Carolina State University.

other elements indicate that they more or less follow the noncarbonate component (Liu, 1982).

Correlations between Element Concentrations and the Noncarbonate Content

To study correlations between element concentrations and the noncarbonate content more quantitatively, a least-squares method was used to analyze the data. To perform regression analysis of our sediment samples, some assumptions were made.

First, we assumed simplistically that the chemical compositions of both the carbonate and noncarbonate components remained constant throughout the sedimentary column. In sediments, the noncarbonate fraction includes clay, sand, and any material other than carbonate; thus its composition depends upon the fractional amounts of these components and their composition. In most of our samples, the noncarbonate phase is predominantly clay, although some samples contain sand, volcanic glass, or other materials. Also, the clay composition from different sources may differ (Turekian, 1968; Grim, 1968), and clays have considerable and varying ion exchange ability (Grim, 1968). It was also assumed that the clay particles are in equilibrium with seawater during their deposition.

Second, we assumed that the preponderance of the carbonates was genetically derived from organisms living in the upper seawater layers oxygenated by the contiguous atmosphere (the carbonate component may be biogenic or authigenic in the oceans). The growing carbonate minerals were also assumed to be in equilibrium with seawater.

Third, it was assumed that the source of clay minerals and the composition of seawater have not changed dramatically in the past 70 Ma (the oldest sediment samples cored at Hole 525A were formed ~70 Ma). A mud sample 525A-53-1, 75–76 cm (574.4 m sub-bottom), immediately above the basalt/sediment interface, exhibits a REE content and relative abundance distribution which are similar to those reported in ordinary clays by Wildeman and Haskin (1965). The Wildeman and Haskin results and our data support previous observations that the REE concentrations in pelagic clays from different locations and different ages are quite similar. Besides, our calculations show that the REE concentrations in seawater at the Walvis Ridge provenance have not changed very much in the past 70 Ma, judging by the REE data of Hole 525A sediments (these results will be discussed later). Therefore, the assumptions of constant clay composition and constant seawater composition are reasonable.

In order to determine the element distributions between carbonate and noncarbonate phases, the data were subjected to regression analysis. For a simple two-

component system; $C = a + bF$, where C = element concentration in the sample; F = the fraction of noncarbonate component in the sample; a = the intercept of regression line; and b = the regression coefficient. The intercept of regression line a is the element concentration in the carbonate component.

The standard deviations of a and b were calculated according to standard formulas by Parratt (1961). The results are given in Table 3. For a comparison, the reported element concentrations in sedimentary clay (Turekian and Wedepohl, 1961; Wildeman and Haskin, 1965) are also listed. The correlations between element concentrations and the noncarbonate content for Al, Sr, and La are plotted in Fig. 2 and are discussed below.

1) Ti, Fe, Al, Mg, K, Sc, V, Cr, Zn, and Rb correlate well with the noncarbonate component (correlation coefficient $r > 0.80$). The intercepts (a) of the regression lines pass through zero within $\pm 2\sigma$ error. Correlation coefficients for Co, As, Hf, Ta, and Th range from 0.30 to 0.78 with zero intercepts within $\pm 2\sigma$ error. These results indicate that these elements are essentially present in the noncarbonate phase. The extrapolations for the noncarbonate element concentrations agree well with the average clay concentrations, within a reasonable range.

2) Sr shows a good negative correlation with the noncarbonate content, where its relatively small concentration indicates that it follows Ca in the carbonate phase, as expected. Ba is present in both the carbonate and the noncarbonate phases, with comparable concentrations.

3) The regression lines of the REE yield definite intercept values that are interpreted as being the average REE abundances in the carbonate phases over the past 70 Ma.

4) Mn abundances in the average carbonate phase are indicated by the intercept of 280 ± 60 ppm; Mn shows an average abundance of 1280 ppm in the noncarbonate or clay phase. The latter is a factor of ~4 times less than is observed in average deep sea clay, but falls within the range of Mn abundances reported in a large number of freshwater and marine clay muds (740–38,000 ppm; *Handbook of Geochemistry*, 1978). The much lower average Mn/Fe ratio observed in the Walvis Ridge clay relative to deep sea clays probably reflects the chemical fractionation achieved under the reducing conditions present during the deposition of most of the clay sediments over the Ridge (see a discussion of redox conditions in the REE section following). Reduction of appreciable Mn to the divalent state probably occurred over the Ridge area, whereas in a higher-oxidation environment under "normal" seawater conditions a large fraction of Mn will be oxidized to the tetravalent state and will thereby become more insoluble by enhanced clay absorption and/or formation of Mn dioxides.

Table 3. The correlations between elements and the noncarbonate phase.

Element	Correlation Coefficient r	Intercept a	Regression Coefficient b	Concentration in Noncarbonate Phase	Concentration in Clay[a]
Major elements (%)					
Ti	0.88	0.01 ± 0.02	0.007 ± 0.001	0.71	0.46
Al	0.96; 0.97	0.17 ± 0.09; 0.11	0.059 ± 0.003; 0.06	6.1	8.4
Fe	0.84	−0.5 ± 0.3	0.077 ± 0.008	7.2	6.5
Mg	0.92	0.10 ± 0.05	0.021 ± 0.001	2.2	2.1
Ca	1.00	40.2 ± 0.1	−0.375 ± 0.002	2.7	2.9
Na	0.72	0.47 ± 0.02	0.008 ± 0.001	1.3	4
K	0.93	0.06 ± 0.05	0.022 ± 0.001	2.3	2.5
Cl	0.73	0.79 ± 0.03	−0.007 ± 0.001	0.09	2.1
Minor and Trace elements (ppm)					
Br	0.41	22 ± 1	−0.09 ± 0.03	13	70
Sc	0.94	0.3 ± 0.3	0.17 ± 0.01	17	19
V	0.90	−9 ± 4	1.8 ± 0.1	171	120
Cr	0.85	2 ± 2	0.47 ± 0.05	49	90
Mn	0.63	280 ± 60	10 ± 2	1280	6700
Co	0.30	0 ± 6	0.4 ± 0.2	40	74
Zn	0.91	−3 ± 3	1.21 ± 0.09	118	165
As	0.49	−0.5 ± 0.6	0.07 ± 0.02	6.5	13
Rb	0.88	2 ± 2	0.80 ± 0.07	82	110
Sr	0.85; 0.79	1120 ± 30; 1050	−10 ± 1; −9	120	180
Ba	0.45	300 ± 60	6 ± 2	900	2300
La	0.73; 0.79	8 ± 1; 7	0.25 ± 0.04; 0.26	33	31
Ce	0.77	7 ± 3	0.62 ± 0.08	69	67
Nd	0.65	7 ± 1	0.19 ± 0.04	26	35
Sm	0.76	1.4 ± 0.2	0.044 ± 0.006	5.8	6.2
Eu	0.91	0.28 ± 0.03	0.010 ± 0.001	1.3	1.8
Tb	0.69	0.20 ± 0.04	0.006 ± 0.001	0.8	1.1
Dy	0.66	1.4 ± 0.2	0.032 ± 0.006	4.6	6.9
Yb	0.63	0.7 ± 0.1	0.022 ± 0.004	2.9	2.9
Lu	0.66	0.09 ± 0.02	0.003 ± 0.001	0.4	0.37
Hf	0.67	0.2 ± 0.2	0.049 ± 0.009	5.1	4.1
Ta	0.64	0.1 ± 0.1	0.016 ± 0.003	1.7	1.2
Th	0.78	0.5 ± 0.3	0.067 ± 0.009	7.2	7
U	0.63	0.1 ± 0.1	0.021 ± 0.004	2.3	1.3

[a] Data for REE are taken from Wildeman and Haskin (1965); data for other elements are taken from Turekian and Wedepohl (1961). Ta data from Hamaguchi et al. (1963). Correlations are based on 39 sediment samples; data obtained for 8 different sediment samples (Sample 525A-25-1, 23–24 cm; 525A-26-1, 3–4 cm; 525A-26-1, 62–63 cm; 525A-27-1, 35–36 cm; 525A-28-2, 10–11 cm; 525A-29-4, 10–11 cm; 525A-30-4, 50–51 cm; 525A-36-3, 15–16 cm) and for three duplicate samples; from Sections 525A-26-2, 525A-31-3, and 525A-36-4, in the second batch of analyzed samples were not included in correlation calculations except for Al, Sr, and La. Second values of r, a, and b for these three elements are based on 50 samples. Since 10 of these 11 samples have $CaCO_3$ concentrations of 95–99% (see Table 1), the calculated values in the fifth column are expected to be unchanged appreciably by the exclusion in the correlation calculations of these 11 samples.

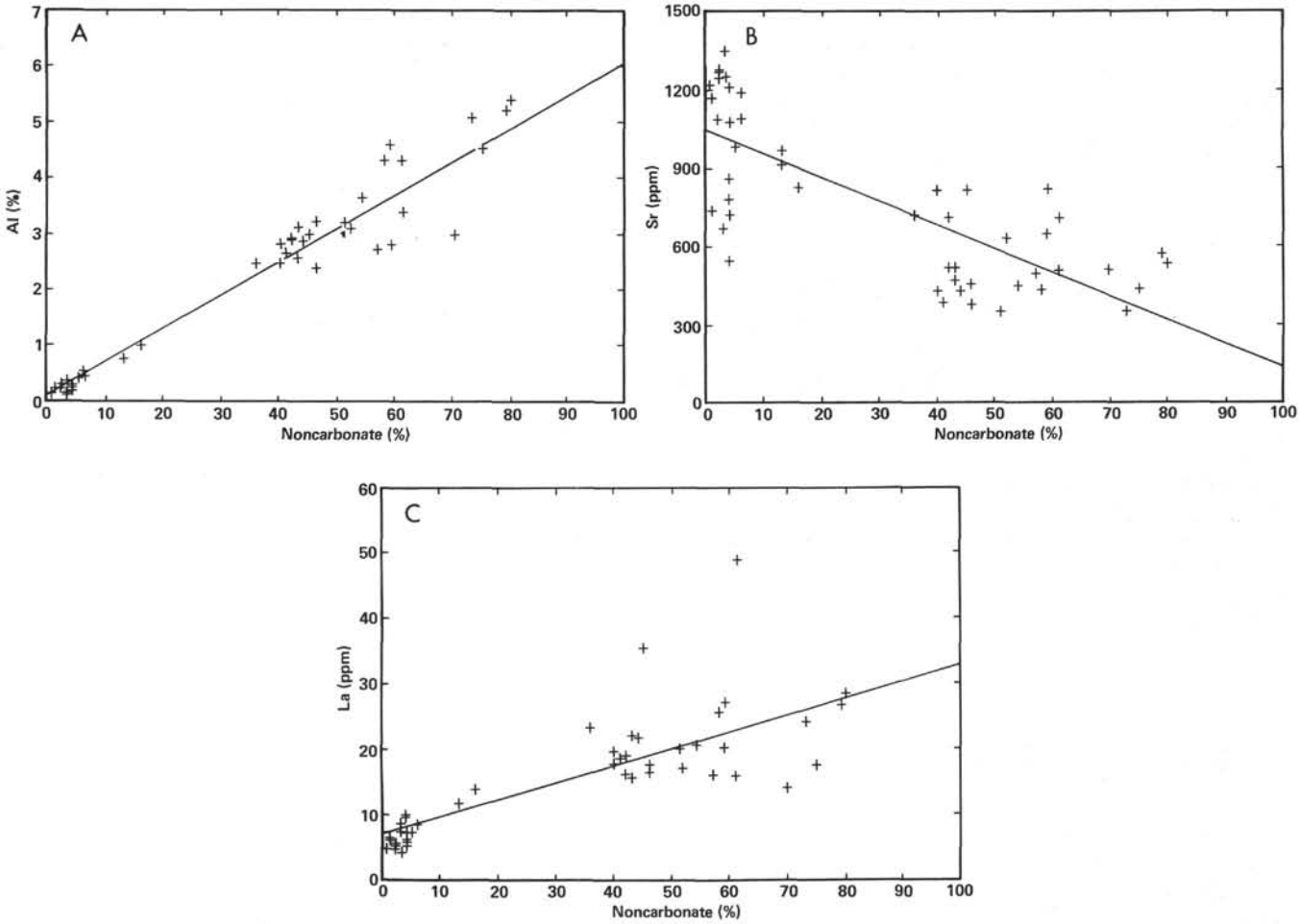

Figure 2. The correlation between the noncarbonate phase in Hole 525A and (A) Al, (B) Sr, (C) La.

The Partition of REE between Calcium Carbonate and Seawater

For a better understanding of the distribution of the REE between carbonate and noncarbonate phases, the partition coefficients of the REE were calculated between seawater and calcium carbonate, as well as in clay. Our assumptions were, first, that the clay particulates achieved equilibrium with seawater with respect to the REE before deposition on the Walvis Ridge floor, and second, that the calcium carbonate was formed biogenically or authigenically in equilibrium with seawater. It was further assumed that after the sediment was deposited, diagenesis did not alter the incompatible-element contents, that is, no appreciable diffusion of trace elements occurred over significant distances. The very high calculated partition coefficients for the REE in carbonate and clay substantiate this assumption.

Assuming that the sediments are composed of two components, carbonate and clay, then the observed concentration, C, of an element in sediments is expressed by:

$$C = F_1 K_1 C_{SW} + (1 - F_1) K_2 C_{SW},$$

where F_1 = the fraction of clay in sediments, K_1, K_2 = the partition coefficients of an element for clay and carbonate, respectively: that is,

$$K_1 = \frac{\text{concentration in clay}}{C_{SW}},$$

$$K_2 = \frac{\text{concentration in } CaCO_3}{C_{SW}},$$

C_{SW} = free ion concentrations in seawater.

The REE concentrations in seawater are taken from Goldberg et al. (1963) and Høgdahl et al. (1968). Turner et al. (1981) calculated the free (uncomplexed) ion fraction in seawater. Because the stability constants were collected from different sources for the calculation of the free ion fractions, considerable deviations may have been introduced in the Turner et al. calculated free ion fractions. The free ion fractions for the REE were obtained from a smooth curve drawn through the calculated REE free ion fractions versus the REE ionic radii. The modified data are listed in Table 4. The data for Ce, Dy, and Lu in brown clay samples were obtained by in-

Table 4. The partition of REE in clay and carbonate phases.

REE	Concentration in Clay[a] (ppm)	Concentration in Seawater[b] (10^{-6} ppm)	Free Ion Fraction in Seawater[c]	Clay Phase K_1 ($\times 10^6$)	Clay Phase K_{1a} ($\times 10^6$)	Carbonate Phase K_2 ($\times 10^6$)	Carbonate Phase K_{2a} ($\times 10^6$)	Carbonate Phase Concentration (ppm)
La	31	3.3	0.38	24	9	3.5	1.4	4.5
Ce	67	1.2	0.27	210	56	10	2.8	3.3
Nd	35	2.7	0.21	61	13	7.9	1.7	4.5
Sm	6.2	0.44	0.18	78	14	9.8	1.8	0.77
Eu	1.8	0.13	0.17	86	14	9.3	1.5	0.19
Tb	1.1	0.14	0.12	65	7.9	8.5	1.0	0.14
Dy	6.9	0.88	0.11	71	7.8	10	1.2	1.0
Yb	2.9	0.78	0.06	61	3.7	14	0.86	0.67
Lu	0.37	0.14	0.05	53	2.6	15	0.76	0.10

[a] From the analysis by Wildeman and Haskin (1965) of three brown clays from the Argentine and Brazil basins. The data for Ce, Dy, and Lu were obtained by interpolation of Ce and Dy between the La and Pr, Nd values and Tb and other HREE values, respectively, and by extrapolation of Lu beyond Yb; all the above are from chondrite-normalized REE ionic radii plots.
[b] From Goldberg et al. (1963), one station, and Høgdahl et al. (1968), six stations; concentration values are weighted by number of stations.
[c] From Turner et al. (1981). Data have been modified according to their ionic radii (see text).

terpolation or extrapolation. From these data, the partition coefficients for clay, K_1, were calculated.

Similarly, the apparent partition coefficients for the total element concentration in seawater have been calculated:

$$K_{1a} = \frac{\text{concentration in clay}}{\text{total element concentration in seawater}}$$

$$K_{2a} = \frac{\text{concentration in carbonate}}{\text{total element concentration in seawater}}$$

Assuming that seawater was in equilibrium with the uppermost analyzed Sample 525A-1-3, 15–17 cm (sub-bottom depth 3.16 m; 98.4% $CaCO_3$) and that it had the same chemical composition as present seawater (probably ~0.3 Ma), the partition coefficients for the REE in the carbonate phase, K_2 and K_{2a}, have been calculated. In these calculations (98.4% $CaCO_3$), corrections were made for the REE concentrations attributed to the calculated 1.6% clay content in the sample. These results are presented in Table 4, as are the REE concentrations in the carbonate phase of the sample.

REE Pattern in the Carbonate Phase

The chondrite-normalized REE concentrations in carbonate of Sample 525A-1-3, 15–17 cm are plotted in Figure 3 as a function of REE ionic radii for the six-coordinated trivalent REE ions. Since the carbonate phase in this sample was presumably derived from largely calcite growth by calcareous nannofossils (~95%) and foraminifers (~5%) and the Ca ion in calcite is six-coordinated, the REE ions are also assumed to occupy a six-coordinated lattice site during calcite growth. The ionic radii are from Whittaker and Muntus (1970). The REE pattern in seawater is also presented in Figure 3.

The major source of REE in the oceans is considered to be rivers that transport weathering products of rocks and soils from the continents. The REE pattern in river water suggests that the erosion of sedimentary rocks, possibly shales, represents the dominant source of REE to seawater (Piper, 1974).

The REE pattern in seawater shows an increase in the concentrations of the heavy REE relative to the REE

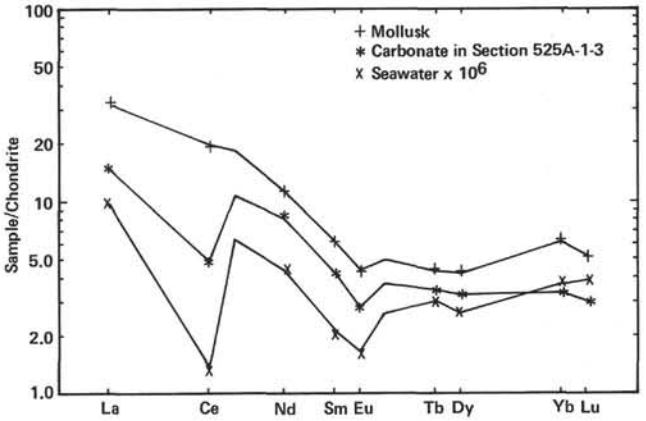

Figure 3. Chondrite-normalized REE concentration patterns of the carbonate phase in Sample 525A-1-3, 15–17 cm, mollusk fragments, and seawater, as a function of six-coordinated ionic radii (Whittaker and Muntus, 1970). Chondrite normalization values in ppm, taken from Ma et al. (1981), are: Rb 2.6, K 650, Ba 3.8, La 0.329, Ce 0.863, Nd 0.620, Sm 0.206, Eu 0.077, Tb 0.046, Dy 0.332, Yb 0.211, Lu 0.036, Sc 7.9, Hf 0.18, Ta 0.022, Th 0.041, and U 0.010. Chondritic values for Rb and K are for the non-volatile fraction of Cl carbonaceous chondrites; chondritic values of Ba, REE, Sc, Hf, Ta, Th, and U are for ordinary CH and CL chondrites. The values of the REE six-coordinated ionic radii are used for Figures 4 and 8 also.

pattern of shale. This monotonic increase is attributed to the greater stability of heavy REE complexes in seawater because of the smaller ionic radii of the heavy REE and hence their greater ionic interactive potential. The marked depletion of Ce in the seawater has been attributed to its oxidation to the tetravalent state in the ocean and its incorporation into the MnO_2 lattice as CeO_2 (Goldberg, 1961; Goldberg et al., 1963). Another mechanism postulates the oxidation of an appreciable fraction of trivalent Ce to tetravalent Ce followed by possible precipitation of highly insoluble hydroxide and its enrichment in some authigenic materials in the ocean (Erlich, 1968). Such a mechanism could be responsible for the striking Ce depletion observed in seawater (Goldberg et al., 1963; Høgdahl et al., 1968). Schmitt (Appendix III in Liu, 1982) has made quantitative calculations on the Ce depletion in seawater and river water and postulated a model to explain the Ce anomalies. The calcula-

tions show that, under the present average Eh of seawater, the concentrations of Ce^{+3} and Ce^{+4} in seawater are controlled by the solubility product of Ce $(OH)_4$. In the present oxidizing seawater environment, the ratio of Ce^{+4}/Ce^{+3} is calculated at $\sim 10^{-15}$; therefore, all soluble Ce in seawater is essentially trivalent. Under river water conditions, further calculations show that all Ce is trivalent, that is, since the solubility product for $Ce(OH)_4$ is not exceeded, all Ce is essentially trivalent.

From these calculations, a simple model ensues. From the weathering of continental rocks, sediments, and soils, all the Ce is Ce^{+3} in river water on its way to the sea. No Ce anomaly is present in the REE pattern of river water. In seawater, an appreciable fraction of Ce is oxidized to Ce^{+4}. From the REE pattern in seawater, one can simply calculate that ~80% of the Ce that enters the oceans is oxidized to Ce^{+4}. The quadrivalent Ce precipitates or coprecipitates as $Ce(OH)_4$, and is occluded or absorbed with flocculating clay particulates and/or precipitated with $Fe(OH)_3 \cdot \times H_2O$ in the seawater, thereby leaving a Ce-depleted REE pattern in seawater. (Similarly, the Eu^{+3}/Eu^{+2} ratio is calculated to be $\sim 10^{15}$ under present seawater redox conditions; very severe reducing conditions are required to reduce trivalent to divalent Eu.) Essentially all carbonates deposited in the oceans are tests of planktonic organisms, such as foraminifers, discoasters, or coccolithophores; the last are by far the most abundant. The carbonates from Section 525A-1-3 to ~560 m sub-bottom range from ooze to indurated nannofossil chalk/limestone with an (~80–95%) nannofossil/20–5% foraminiferal character. As expected, the REE pattern in Sample 525A-1-3, 15–17 cm shows a Ce depletion. The heavy REE in the carbonate show a slight decrease compared to the REE pattern of seawater.

Spirn (1965) measured the REE in several *Globigerina* tests sampled from an equatorial Atlantic core, and Turekian et al. (1973) measured REE concentrations in several species of pteropods. Our results, consistent with these works, show similar REE patterns with a Ce depletion. The REE pattern in biogenic carbonate simply reflects that in seawater, that is, the incorporation of the available trivalent REE into the growing carbonate lattices (calcite or aragonite) of the organisms.

The Partition Coefficients of the REE

The K_1, K_{1a}, K_2, and K_{2a} are shown in Figure 4 as a function of the six-coordinated trivalent REE ionic radii.

The partition coefficients of the free REE ions in the carbonate phase, K_2, increase monotonically with a decrease of trivalent REE ionic radii. Because of the lanthanide contraction, the heavy REE have increasingly smaller ionic radii and consequently the smaller REE are expected to form stronger bonds in the calcite lattice, thereby exhibiting an increase in the K values. For clay, the partition coefficients K_1 increase from La to Eu, and then decrease slightly from Tb to Lu. Undoubtedly, the complexity of the clay structure and sites and the absorption properties of the REE flatten out the heavy REE pattern.

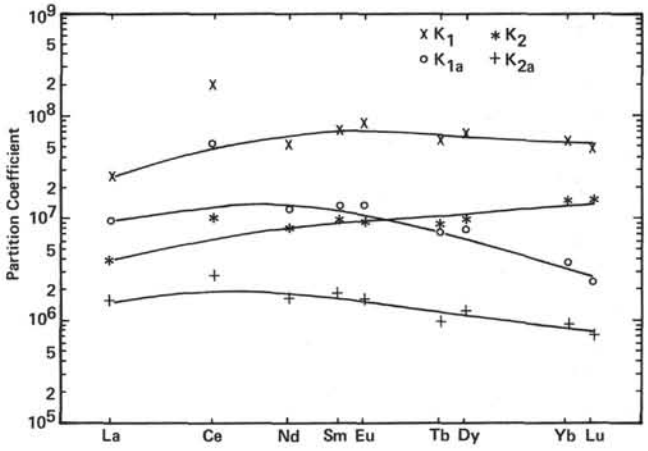

Figure 4. The partition coefficients of REE between carbonate, clay, and seawater as a function of six-coordinated ionic radii. Symbols K_1 and K_2 are REE concentrations in clay and in $CaCO_3$, respectively, as a proportion of free REE ion concentrations in seawater; K_{1a} and K_{2a} are REE concentrations in clay and in $CaCO_3$, respectively, as a proportion of total REE concentrations in seawater.

The apparent partition coefficients for clay K_{1a} and carbonate K_{2a} both pass through a maximum around Ce and Nd. Because of the lanthanide contraction, the bonds of the REE ions become stronger when the atomic number increases, and consequently stronger complexes with anions such as $CO_3^=$, $SO_4^=$, and Cl^- are formed in seawater by the heavier REE; therefore, the free REE ion concentrations decrease with increasing atomic number (see Table 4, col. 4). The total effect makes the apparent coefficients K_{1a} and K_{2a} increase slightly from La to Ce and then decrease.

The partition coefficients of Ce appear higher than would be expected from the properties of trivalent REE. However, since the K_2 and K_{2a} values were calculated by including a subtractive term that accounts for the small fraction (with an associated uncertainty) of noncarbonate matter in Sample 525A-1-3, 15–17 cm and since that subtractive term is relatively more significant for the final K_2 values of Ce relative to the K_2 values for La and Nd, the higher K_2 and K_{2a} values of Ce above the smooth K_2 and K_{2a} curves may be unreal. In summary, within the experimental uncertainties, the Ce points for K_2 and K_{2a} probably lie on a smooth La–Ce–Nd pattern (Fig. 4). As expected, the K_1 and K_{1a} values for clay are significantly higher than the corresponding K_2 and K_{2a} values for $CaCO_3$.

Parekh et al. (1977) used regression analysis to obtain REE concentrations in the carbonate phase for marine limestone samples from southern Germany. Their results show similar REE patterns with Ce depletions and similar partition patterns of REE between $CaCO_3$ and seawater.

The REE partition coefficients in $CaCO_3$ are high, and are even higher in clay. Because the REE form relatively insoluble carbonates (e.g., the K_{sp} values for $Pr_2(CO_3)_3$ and $Nd_2(CO_3)_3$ are 10^{-27}; Sillen et al., 1971), the high partition coefficients for REE in the $CaCO_3$ lattices are entirely in line with K. Fajans' principle. This

has practical importance for radioactive waste disposal. Shanbhag and Morse (1982) have determined the distribution coefficient of 433-y Am^{+3} between calcite and seawater and found the lower limit to be $\geq 2\times10^5$. Since the ionic radius of Am^{+3} is close to that of Nd^{+3}, their chemical properties are very similar. Consequently, the lower limit of 2×10^5 for ^{241}Am is consistent with our apparent partition coefficient value for Nd^{+3} in calcite/seawater of 1.7×10^6. Since the ionic radius of Pu^{+3} is close to that of Ce^{+3}, the apparent partition coefficient for Pu^{+3} may be close to that of Ce^{+3} ($\sim1.9\times10^6$). The partition coefficient for Pu^{+4} should be even higher, like Ce^{+4}. Very likely, a large fraction of Pu^{+4} is precipitated as the insoluble $Pu(OH)_4$ state analogous to appreciable Ce^{+3} oxidation to $Ce(OH)_4$. Carpenter and Beasley (1981) have determined the distributions of Pu and Am in sediments from anoxic basins. They found that there is no rapid remobilization of Pu and Am. Our results show an extremely high affinity of lanthanides for $CaCO_3$ and clay; considering the chemical similarity between lanthanides and actinides, it is easy to understand the results of Carpenter and Beasley even in anoxic marine sediments, where Pu is present largely in the trivalent state.

La Concentration in Seawater during the Past 70 Ma over the *Walvis Ridge*

If we use the REE partition coefficients for $CaCO_3$ and clay at the present time to calculate the REE concentrations over the past 70 Ma, deviations will provide some information about changes in the REE concentrations and about seawater compositional changes in general. Changes in the concentration in seawater of La, as a typical light REE, are presented in Figure 5. The average La concentration in seawater obtained from the La data in 37 sediment samples is $(3.4\pm0.8)\times10^{-6}$ ppm ($\pm1\sigma$) which agrees well with that measured by Goldberg et al. (1963) and Høgdahl et al. (1968) in modern seawater. Of the 39 data points in Figure 5, Samples 525A-45-4, 53–54 cm and 525A-46-3, 22–23 cm were not included in the calculation of the above-average La concentration in seawater, because their composition corresponds largely to that of volcanic glass. The La concentration has not changed much over the past ~70 Ma at this site. This result is striking because the residence time of lanthanides in the ocean is short, only < ~300 y. (Goldberg et al., 1963; Wildeman and Haskin, 1965). The partition coefficients are also affected by bulk composition. Therefore, this result also implies that the bulk composition of seawater and the clay, $CaCO_3$, and other particulates in the sediments has been quite constant over the past 70 Ma, a relatively short span of geologic time. In view of the fact that the $CaCO_3$ fraction in these 37 sediment samples ranged from 0.01–0.99, it seems very unlikely that particulates such as fish bone debris, even in small fractional amounts, could be responsible for the high calculated REE partition coefficients of $CaCO_3$. To obtain such uniform La concentrations in seawater with a *broad* range of $CaCO_3$ fractions would demand a nearly constant ratio of $CaCO_3$ to fish bone debris over the past 70 Ma; such a proposition does not seem realistic.

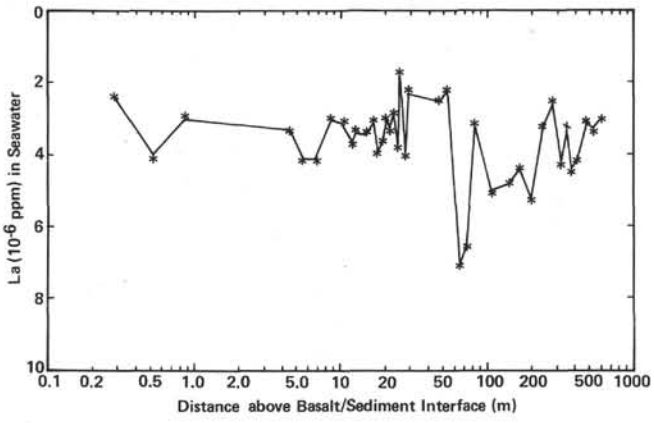

Figure 5. The La concentrations in seawater which were in equilibrium with sediments formed over the past 0.3–70 Ma on the Walvis Ridge. The two high calculated La concentrations at $\sim7\times10^{-6}$ ppm are unreal because these two samples (525A-45-4, 53–54 cm and 525A-46-3, 22–23 cm) correspond largely to a volcanic glass composition. La concentration calculations were based on the 39 sediments of the first group of analyzed sediments (see Activation and Counting section of text).

Volcanic Glasses in Sample 525A-46-3, 22–23 cm

Figures 1C and 5 exhibit higher La concentrations in Samples 525A-45-4, 53–54 cm and 525A-46-3, 22–23 cm relative to other samples. The REE patterns and those of some other elements for Sections 525A-44-4 to 525A-47-4 are plotted in Figure 6. Since the structure of clay is not well understood, it is assumed that the REE are eight-coordinated in clay absorption. Samples 525A-45-4, 53–54 cm and 525A-46-3, 22–23 cm show more Eu depletion, and the relative abundances of K, Rb, and Ba are also lower than "normal" samples, suggesting they were derived from different sources. Volcanic glasses also exist in sediments of the same age at Sites 528 and 529, which are close to Hole 525A. There are no volcan-

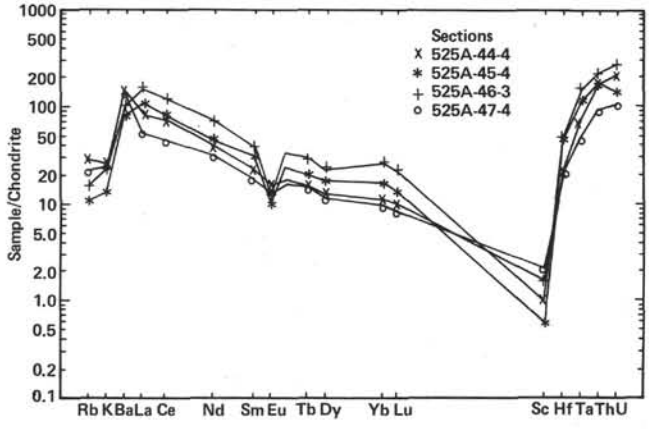

Figure 6. Chondrite-normalized element concentration patterns of Hole 525A samples. REE and Sc units are in decreasing eight-coordinated ionic radii (Shannon, 1976).

ic ash falls or breccias found at Site 363, Leg 40, at the Walvis Ridge (Ryan et al., 1978). The age of the oldest sediments cored at this site is early Aptian. A mid-Eocene volcanic–sedimentary breccia was found at the Rio Grande Rise (Site 357, Leg 39) (Fodor and Thiede, 1977). Late Eocene tuff was found at the Walvis Ridge seamount (Site 359, Leg 39) (Fodor, Keil, et al., 1977). These facts suggest that the volcanic activities were localized and that the volcanic activity which formed the volcanic glass at Hole 525A was nearby. The age of Sample 525A-46-3, 22–23 cm is estimated at ~67 Ma. It is assumed that this section of the Walvis Ridge was formed near the mid-ocean ridge spreading center ~70 Ma, and that the spreading rate was ~2 cm/y. Therefore, the mid-ocean ridge spreading center was ~60 km away to the west at that time. It is interesting to note that the Walvis Ridge at Site 363 was formed during the Aptian; if there were any recorded volcanic activity, it should have occurred before the early Aptian. Site 359 on the Walvis Ridge seamount was formed ~50 Ma. It recorded volcanic activity at ~40 Ma (Fodor, Keil, et al., 1977). All these volcanic activities occurred when these sites probably were close to the mid-ocean spreading center, implying that most volcanic activities occurred at or near the spreading center.

Sample 525A-46-3, 22–23 cm is a mixture of carbonate, clay, volcanic glass, palagonite, and the like. It is difficult to determine the original volcanic glass composition. The high enrichment of the light REE indicates that it is not related to ocean floor tholeiitic basalt, but could be associated with an explosive, oceanic-island, alkalic basalt type. The basement basalt of this site, Sample 525A-63-1 (Piece 2A), is similar to an oceanic island alkalic basalt. However, in Sample 525A-46-3, 22–23 cm, higher abundances of Rb, Yb, Lu, Hf, Ta, Th, and U, a lower Sc abundance, and a negative Eu abundance are found relative to the "fresh" basement basalt, 525A-63-1 (Piece 2A), (compare Figs. 6 and 10, later). Quite possibly, the volcanic glass may have a composition similar to a more silicic rock like andesite or dacite (such as at Site 359; Fodor, Keil, et al., 1977). Either the source matter from which the volcanic glass was derived by partial melting had plagioclase and pyroxene as residual minerals to account for the lower Eu and Sc abundances, or plagioclase and pyroxene crystallization occurred in the magma chamber before the explosive eruption of the volcanic glass.

Ce Anomaly in Sediments: The Time When the Ocean Water Became Oxidizing over the Walvis Ridge

We have discussed previously in this paper the Ce depletion in biogenic carbonate which reflects the Ce^{+3} depletion in seawater. If seawater is in a reducing state, all Ce will be trivalent and will follow other normal trivalent lanthanides, resulting in a normal REE pattern in biogenic carbonate. If seawater is in an oxidizing condition, Ce will be depleted to varying degrees in the water, resulting in a Ce-depleted REE pattern in carbonate. Consequently, the REE pattern in biogenic carbonate is an important redox indicator of primarily surface seawater.

A mollusk (*Inoceramus*) shell segment sample from upper Campanian sediments (~70 Ma) has been analyzed. The REE pattern in the carbonate shell of this shallow-water (<200 m) benthic organism is shown in Figure 3. It has essentially the same REE pattern as observed in Sample 525A-1-3, 15–17 cm (98% carbonate), except that no Ce anomaly was found in the mollusk sample. This result indicates that the relative abundances of REE (Ce excepted) in seawater were essentially the same as in the present seawater. The more open aragonitic $CaCO_3$ structure in *Inoceramus* accounts for the fact that light and heavy REE concentrations are ~2.5 and ~1.5 times higher, respectively, in *Inoceramus* relative to the more closed calcitic $CaCO_3$ structure in the foraminiferal–nannofossil carbonates that predominantly compose Sample 525A-1-3 15–17 cm and others in Hole 525A. A normal Ce pattern in the mollusk carbonates indicates that seawater redox conditions at this provenance were anoxic in the late Campanian at the shallow benthic levels for *Inoceramus* growth.

The Mn content of 2110 ppm in the ultrasonically cleaned mollusk fragments suggests that some Mn oxide surface contamination may be present and may contribute some REEs to the REEs indigenous to the carbonate phase. We note that the Mn content in ≥95% of the calcium carbonate samples is ~150 ppm (e.g., see Mn in Sample 525A-1-3, 15–17 cm) in modern (~0.3 Ma) oxidizing seawater. Assuming that all the Mn present in the mollusk sample has a composition like that of a Mn-oxide nodule, the maximum Mn-nodule matter is ~1%. From the average Co content in Mn nodules (~1500 ppm), we calculate that Mn-nodule–like contamination of the mollusk is ~0.3%, maximum. Assuming ~100 ppm La, ~400 ppm Ce, and 34 ppm Sm in an average Mn nodule (Elderfield and Greaves, 1981), we calculate that, at a maximum, La, Ce, and Sm amounts of ~0.3 ppm, ~1.2 ppm, and ~0.1 ppm, respectively. The mollusk sample can be attributed to Mn-nodule–like contamination of ~0.24%. Subtraction of these upper contamination limits will not significantly change the observed normalized REE pattern (Fig. 3) nor any conclusions. But it is also likely that the Mn may be present as a Mn-oxide coating produced by diagenesis in the sedimentary column. Because of the very high REE partition coefficients for the surrounding clay material, limited REE diffusion could result in an Mn oxide low in REE and thus in minimum REE contamination of the REE indigenous to the mollusk carbonate.

Since the final residence depth of the *Inoceramus* in the sedimentary column was 2467 m of seawater and 550 m of overlying sediment, it is very likely that the aragonitic structure of *Inoceramus* was not transformed to the calcitic structure via recrystallization. Even if some restructuring occurred, the high partition coefficients of REE in calcite would prevent diffusional loss of REE from the carbonate lattice.

From perusal of the graphic lithologies of Cores 525A-50 and 525A-51, where the *Inoceramus* fragments are most abundant (Boersma, this volume), it appears that the *Inoceramus* grew largely on a nannofossil chalk platform, probably located on the shelf margin of the

Walvis Ridge. From our studies of Core 525A-50 (545–555 m downcore), we calculated that the carbonate fractions in 7 representative core samples range from 0.32–0.60 (Table 1) whereas in Core 525A-51 (555–564 m downcore), the carbonate fractions in 6 representative samples range from 0.29–0.60. Correspondingly, the noncarbonate (assumed to be a largely clayey component) fractions range from 0.68–0.40 and 0.71–0.40, respectively, in Cores 525A-50 and 51. However, it is conceivable that reducing conditions resulted from the presence of organic debris in the mud and pore water exposures at the benthic levels of *Inoceramus* growth. In such an event, the absence of a depleted Ce anomaly in the mollusk carbonate would not necessarily reflect the surface seawater redox conditions, which could very likely also have been reducing—see later. In any case, such an interpretation does not apply to differences observed in the Ce anomalies in two ≥96% $CaCO_3$ Samples 525A-30-4, 50–51 cm and 525A-31-3, 5–6 cm (see later).

It is desirable to ascertain when ocean water became oxygenated to its present redox condition. Figure 7 exhibits the downcore profile of the La/Ce ratio. Figure 8 shows the REE patterns of Samples 525A-1-3, 15–17 cm,

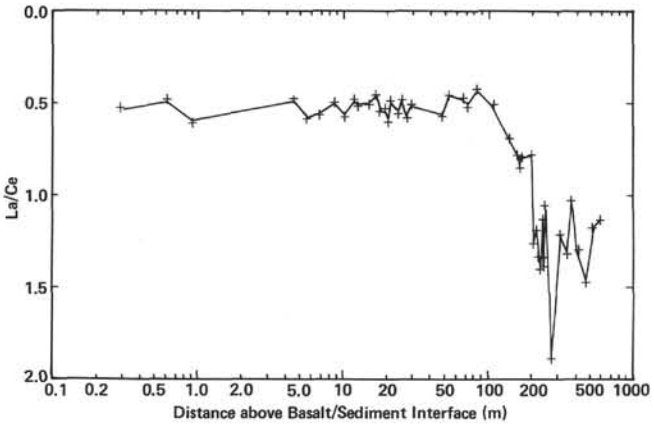

Figure 7. The downcore profile of the La/Ce ratio in Hole 525A.

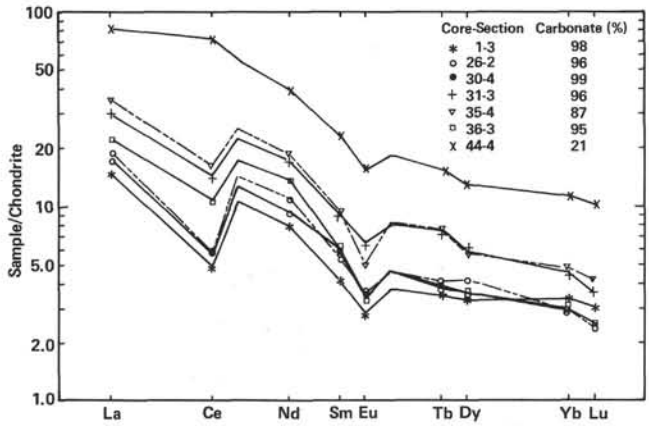

Figure 8. Chondrite-normalized element concentration patterns of Hole 525A samples. REE units are in decreasing six-coordinated ionic radii.

525A-26-2, 84–85 cm, 525A-30-4, 50–51 cm, 525A-31-3, 5–6 cm, 525A-35-4, 130–131 cm, 525A-36-3, 15–16 cm, and 525A-44-4, 50–52 cm, with carbonate contents ranging from 98–87%. Bender et al. (1971) analyzed a predominantly calcite sample from a core from the slope of the mid-ocean East Pacific Rise and found a lanthanide distribution similar to that observed in the carbonate Sample 525A-1-3, 15–17 cm. Kyte et al. (1980) analyzed via INAA three carbonate-rich samples (calcareous nannofossil–foraminiferal ooze with $CaCO_3$ of 66–100%) taken from DSDP Hole 465A, Core 3 (Central Pacific, 33°49.23′N, 178°55.14′E). In all three samples, the lanthanide distributions were similar to that observed in the REE pattern for Sample 525A-1-3, 15–17 cm, with an even more pronounced Ce depletion in the Central Pacific oozes. Concentrations of other trace elements in Sample 525A-1-3, 15–17 cm (>96% $CaCO_3$) and in the ~100% $CaCO_3$ sample from the Central Pacific core agree well; this again confirms the relative uniformity of composition of surface seawater. Samples 525A-1-3, 15–17 cm to 525A-31-3, 5–6 cm and 525A-36-3, 15–16 cm contain only a few percent (≤4%) of a noncarbonate component. Since their REE patterns are dominated by the carbonate phase, one can infer whether Ce is depleted in carbonate. The noncarbonate components in Samples 525A-35-4, 130–131 cm and 525A-38-3, 119–120 cm are higher and the Ce depletion seems to be present, but less certainly. In deeper cores, for example Section 525A-44-4, the noncarbonate contents are much higher (e.g., 70% in Sample 525A-44-4, 50–52 cm), and therefore the REE patterns are dominated by clay in which Ce is not depleted. From such core samples with a high clay component, it is impossible to ascertain whether or not Ce was depleted in the carbonate phase. Fortunately, the data in Figures 7 and 8 show that a dramatic change in Ce depletion occurred between Section 525A-30-4 (~205 m above the basalt/sediment interface; Fig. 8) and 525A-31-3 (~198 m above basalt/sediment interface; Fig. 8). We emphasize that Sample 525A-30-4, 50–51 cm exhibits the same Ce depletion as observed in the most recent carbonate sample such as 525A-1-3, 15–17 cm, indicating that since the early Eocene the surface ocean water over the Walvis Ridge has been in an oxidizing condition similar to that at present. Since the 96% carbonate Sample 525A-31-3, 5–6 cm shows much less Ce depletion relative to the 97% carbonate Sample 525A-30-4, 50–51 cm, we suggest that during the time that core segment 525A-31-3 was deposited, only a small fraction of Ce was oxidized to the quadrivalent state. Sections 525A-35-4, 525A-36-3 and 525A-38-3 also show evidence of redox conditions similar to those inferred for the deposition of Section 525A-31-3. As noted above, the REE patterns of deeper sedimentary samples are dominated by a noncarbonate component, thereby precluding inferences about the seawater redox conditions *via* Ce depletion. Interpretation of the REE pattern of the mollusk suggests that seawater was anoxic in the late Campanian at shallow benthic levels (note the possibility of enhanced anoxic conditions in the growing *Inoceramus* environment as discussed earlier), and this is consistent with the change in reducing to oxidizing condi-

tions that is suggested by the differences in Ce depletions in Samples 525A-31-3, 5–6 cm and 525A-30-4, 50–51 cm. In conclusion, we suggest that sometime between the Maestrichtian and the early Paleocene seawater started gradually becoming less anoxic. During the deposition times for Sections 525A-31-3 and 525A-30-4 (late Paleocene), ~54 Ma, the surface seawater over the Walvis Ridge became oxygenated like present seawater.

The Walvis Ridge and the São Paulo Plateau–Rio Grande Rise complex obstruction were the major factors for maintaining stagnant and anoxic waters in the Angola–Brazil Basin. The oldest sediments cored in Hole 525A were deposited during the late Campanian, very close to the age of the basement rocks. Sediments derived from shallow water suggest that the Walvis Ridge was just below sea level at that time and prevented good circulation between the Cape and Angola basins. Subsequently, the Walvis Ridge subsided. On the west side of the mid-ocean ridge, the Rio Grande Rise subsided below sea level during the Campanian (Supko, Perch-Nielsen, et al., 1977a). Better water circulation was achieved during the Late Cretaceous and Paleocene. We hypothesize that during late Paleocene times (~54 Ma) the Walvis Ridge and the Rio Grande Rise subsided far enough to explain the increased carbonate production (~96%) observed in Sections 525A-30-4 and 525A-31-3. Also, we hypothesize that the water passage between northeast Brazil and west central Africa (near present-day Liberia) was apparently wide enough ~54 Ma because of the continued continental drift to allow a circulation between the North and South Atlantic sufficient to achieve redox conditions over the Walvis Ridge that are similar to present conditions. The hypothesized map of ~54 Ma is illustrated in Figure 9.

The time of ~54 Ma is much later than the Late Cretaceous age of ~70 Ma suggested by Natland (1978) and Bolli, Ryan et al., (1978a). This difference could be attributed to different criteria for describing the redox condition over the Walvis Ridge. Some observations are based on the presence of carbonaceous material, some based on the color of sediments, that is, the oxidation state of Fe. The hypotheses of this chapter are based on the oxidation state of Ce, which differs from the redox potential of iron. It is also possible that the anoxic or oxygenated condition might be a localized phenomenon in some areas.

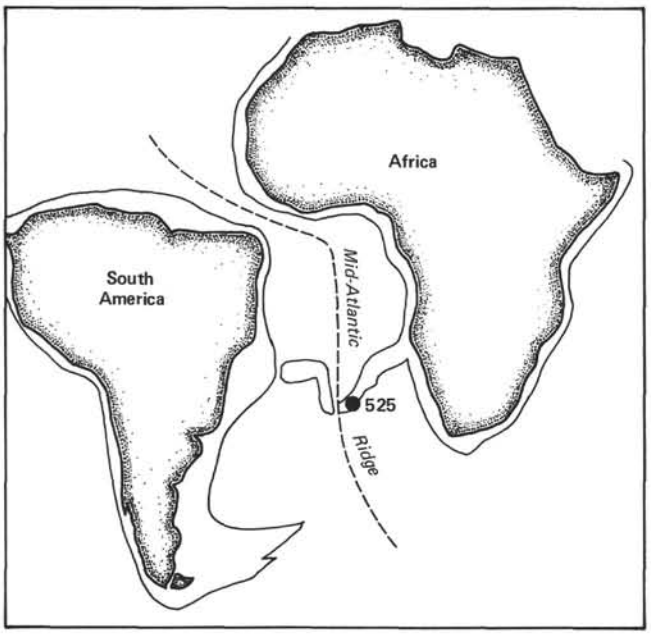

Figure 9. Sketch of the relative position of South America and Africa, ~54 Ma.

The Basement Basalts

Four basalt samples generated during the Campanian (525A-53-1 [Piece 1D] to 525A-63-1 [Piece 2A]), ~70 Ma (Richardson et al., 1982), were analyzed. Samples 525A-53-1 (Piece 1D) and 525A-53-3 (Piece 7A) are from the same basalt layer. Samples 525A-58-2 (Piece 2H) and 525A-63-1 (Piece 2A) were taken from separate layers. The last sample was only slightly altered; the others were moderately to extensively altered. Their patterns of REE plus some other elements are presented in Figure 10. To check the possibility of major, minor, and trace element losses resulting from seawater leaching of the only slightly altered basalt 525A-63-1 (Piece 2A), two aliquants of the sample were subjected to INAA. One sample was analyzed as received; the other sample was subjected to dissolution of weathered products by a 5 min. 0.1N HCl treatment before activation. The INAA results indicate insignificant chemical weathering losses in the original, slightly altered sample that are consistent with our understanding of bulk, accessory, and secondary mineral sites of trace and bulk elements in unweathered rocks.

There have been several sites drilled on the Walvis Ridge, São Paulo Plateau, and Rio Grande Rise. Bolli, Ryan, et al. (1978b) studied Sites 362 and 363, Leg 40. Site 362 is located on the Frio Ridge segment of the Walvis Ridge where it joins the continental margin of Southwest Africa. At Site 362, the inferred basalt basement was not reached. The nearby Site 363 was located at an isolated basement high on the north-facing escarpment of the Frio Ridge portion of the Walvis Ridge. Here,

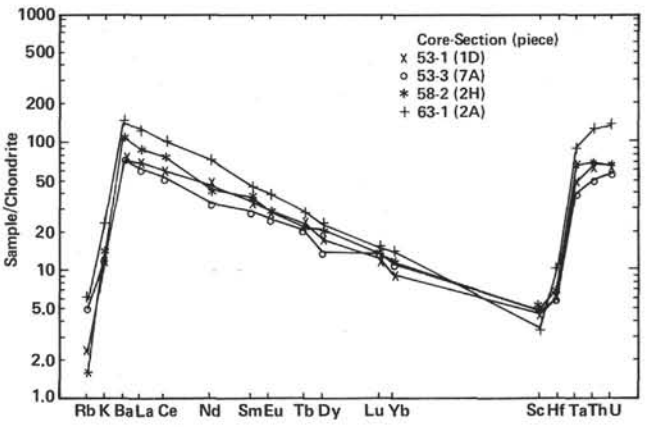

Figure 10. Chondrite-normalized element concentration patterns of basement basalt samples, Hole 525A. REE and Sc are in units of eight-coordinated ionic radii.

also, the basalt basement was not penetrated. Presumably, the Frio Ridge was created near the mid-ocean ridge during the Aptian (~110 Ma), according to magnetic anomaly measurements. The first rocks found in a nearby dredge haul have been reported by Hekinian (1972), who suggests that at one time elevated submarine volcanos were active near the continental margin of Southwest Africa.

The age of the seamount on the western part of the Walvis Ridge is supposed to be 50 Ma. The trachytic tuff on the top of the seamount resembles the volcanic rocks on the nearby islands of Tristan da Cunha and Gough. A K-Ar age for feldspar in the trachyte indicates it was emplaced ~40 Ma (Supko, Perch-Nielsen, et al., 1977a; Fodor, Keil, et al., 1977).

Tracing the Walvis Ridge closer to the mid-ocean ridge leads to the island Tristan da Cunha, which is ~18 Ma old and has been proposed as the locus of the current Walvis Ridge–Rio Grande Rise "hot spot" (Wilson, 1963). The volcanic rocks of the Tristan da Cunha and Gough islands have also been studied (Baker et al., 1962; LeMaitre, 1962).

The São Paulo Plateau–Rio Grande Rise Complex is the presumed counterpart of the Walvis Ridge in the southwestern Atlantic. Site 357, Leg 39, is on the Rio Grande Rise. The age of basement rocks is suggested to be 97 Ma (Supko, Perch-Nielsen, et al., 1977b). Fodor, Husler, et al. (1977) have studied rock samples, dredged from the Rio Grande Rise, that have the compositional characteristics of an alkalic basaltic suite, not of MORBs. The age of basement rocks at Site 356 on the São Paulo Plateau is suggested to be between 110 and 127 Ma (Supko, Perch-Nielsen, et al., 1977c). The average bulk chemical compositions of basalts from the eastern end of the Walvis Ridge (Hekinian, 1972), Tristan da Cunha Island (Baker et al., 1964), Gough Island (LeMaitre, 1962), Rio Grande Rise (Fodor, Husler, et al., 1977), and the Mid-Atlantic Ridge (Engel and Engel, 1964), as well as of Sample 525A-63-1 (Piece 2A) are summarized in Table 5.

Engel et al. (1965) have compared the average compositions of oceanic tholeiitic basalts with alkali basalts from seamounts and islands. The oceanic tholeiites have 45–50% weight silica, a lower ratio of Fe_2O_3/FeO in the unaltered rock, a higher ratio of Na/K, and lower concentrations of Ba, K, P, Rb, Sr, Ti, and Zr. Oceanic tholeiites also contain only small abundances of Th, U, and Pb (Tatsumoto et al., 1966). Based on these characteristics, the values for K, Ti, Sr, Ba, Th, and U (Table 2) in basalt Sample 525A-63-1 (Piece 2A) indicate alkali basaltic affinities like other basalts on the Walvis Ridge, oceanic islands, and the Rio Grande Rise (Table 5).

Oceanic island basalts have strikingly different lanthanide distributions than do the MORBs. They show strong relative enrichments with increasing REE ionic radii, whereas the MORBs are depleted in light REE (e.g., Haskin and Paster, 1979). In Figure 10, Sample 525A-63-1 (Piece 2A) shows a strong enrichment of the light REE. Samples 525A-53-1 (Piece 1D), 525A-53-3 (Piece 7A), and 525A-58-2 (Piece 2H) are moderately to extensively altered and exhibit lesser light REE enrichments than 525A-63-1 (Piece 2A). The chemical compositions of Site 525A basement rocks are definitely those of oceanic-island alkalic basalts, not MORBs.

If we assume that the basalts in Hole 525A were derived by similar degrees of partial melting from the same mantle source rock, and if we further normalize the lanthanide patterns of Samples 525A-53-1 (Piece 1D) to 525A-63-1 (Piece 2A) (Fig. 10) to the same Yb and Lu + Sc abundances—these heavy REE + Sc will be leached least among the REE + Sc—we observe that the REE from Dy to La have been leached to increasing degrees. The data indicate as much as ~30–50% leaching of the light REE, Ba, Hf, Ta, Th, and U in the extensively weathered basalts in Core 53 relative to the lightly altered basalt Sample 525A-63-1 (Piece 2A). Plotting the log of the chondrite-normalized values for the REE and Sc versus their eightfold coordination number yields a straight line of the kind expected from a partial melting event for basaltic generation. Such similar REE + Sc patterns have been observed for a large number of Mount St. Helens' recent andesitic ash and dome samples (Hughes, S., and Smith, M. R., pers. comm., 1981). The absence of a preferential loss of U relative to Th in the extensively altered Core 525A-53 basalts suggests that reducing conditions in the seawater prevented appreciable oxidation of U to the uranyl state; consequently, the tetravalent Th and U exhibited similar weathering behavior for leaching and absorption phenomena.

The time sequence for the formation of the Walvis Ridge from Sites 362, 525, and 359 to the islands Tristan da Cunha and Gough indicate that younger rocks are closer to the mid-ocean ridge. The São Paulo Plateau–Rio Grande Rise complex shows a similar time sequence,

Table 5. Basalt compositions of major elements (in %) at Walvis Ridge and related sites.

Element	Eastern Walvis Ridge (Hekinian, 1972)	Sample 525A-63-1 (piece 2A), Walvis Ridge	Tristan da Cunha Island (Baker et al, 1964)	Gough Island (LeMaitre, 1962)	Mid-Atlantic Ridge (Engel and Engel, 1964)	Rio Grande Rise (Fodor, Husler, et al., 1977)
SiO_2	49.5	—	43.1	47.7	49.9	49.0
TiO_2	2.9	3.2	3.6	3.2	1.2	2.8
Al_2O_3	16.0	16.5	13.1	15.2	17.3	15.7
Fe_2O_3	10.3	—	5.5	2.3	1.9	6.1
FeO	2.3	9.1[a]	8.5	8.7	7.0	2.5
MgO	2.8	4.3	9.0	9.7	7.9	5.1
CaO	6.8	7.8	12.4	8.9	11.5	7.8
Na_2O	2.8	3.9	1.6	2.7	2.8	3.7
K_2O	2.3	1.9	3.6	1.6	0.16	3.2

Note: A dash indicates that the element was not detected.
[a] All Fe expressed as FeO.

though fewer data are available. Wilson (1963, 1965) and Morgan (1971, 1972) have suggested that the Walvis Ridge and São Paulo Plateau–Rio Grande Rise complexes consist of a chain of volcanos which grew over a "hot spot" near the mid-ocean ridge and then were carried by both sides as seafloor spreading. The bulk chemical data that are presented in Table 5 do not refute such a hypothesis.

Comparison of Basalts On and Near South America and Hole 525A Basement Basalt

Nine basalt samples from southern and offshore Brazil were analyzed by INAA. Among them, two samples (PAR-1 and PAR-2), are Paraná basalts, and two are from holes drilled by Petrobrás along the coastline of Espírito Santo, southeast Brazil. Five samples were recovered from offshore drill holes along the southeastern margin of Brazil (Fig. 11). The two Paraná basalts were obtained from G. Meeker and the other Brazilian samples from R. V. Fodor.

PAR-1 and PAR-2 basalts have been discussed by DePaolo and Wasserburg (1979). Both samples are from a drill core near Santa Catarina in Brazil (49°55′W, 28°46′S) and have K-Ar ages of 120 Ma PAR-1 is from the base of the section (elevation 300 m) and PAR-2 is from higher in the section (elevation 750 m). The major element compositions of these two samples (Table 2) are fairly close to the average composition of Parana basalts cited in Herz's paper (1977). The REE and other trace element patterns of these two samples are different (Fig. 12). Also, the concentrations of Cr and Sr are higher in PAR-1 than in PAR-2, and Co is high in PAR-2 (Table 2). The composition of PAR-1 is very similar to that of Sample 525A-63-1 (Piece 2A), including the REE pattern (compare Figs. 10 and 12). When Paraná basalt formed 120 Ma, the Paraná province was near the mid-ocean spreading center. The Hole 525A section of Walvis Ridge formed ~50 Ma later. Apparently, over a time span of ~70 Ma, very similar source matter from the mantle was partially melted to similar degrees to yield the continental Paraná basalts and the Walvis Ridge basalts. Such an observation questions the uniqueness of the chemical composition of "hot spot" mantle matter relative to the source matter in the mantle from which continental basalts are derived.

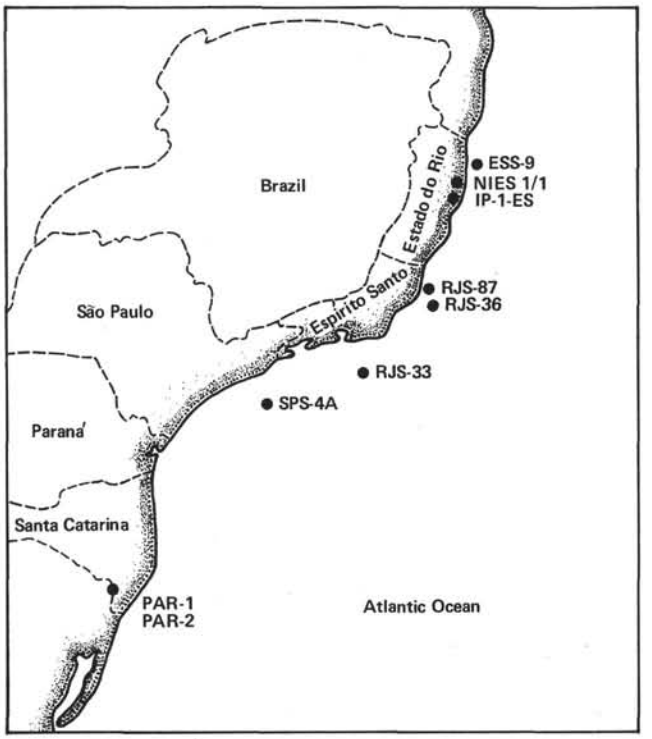

Figure 11. Sketch of basalt core locations along the Brazil coast.

The patterns of the REE and several other elements of sample NIES 1/1 and 1P-1-ES are also shown in Figure 12. The overall trace element pattern for the NIES 1/1 basalt matches quite closely the PAR-1 sample; however, there are significant differences for some major, minor, and trace elements for these two samples. The basalt 1P-1-ES is a low-alkali basalt with a REE pattern intermediate between MORBs and alkalic basalts.

There are five samples taken from the continental margin of Brazil. Geophysical data suggest that the boundary between continental and oceanic crust is present beneath and near the edge of the continental shelf off Brazil (see Kowsmann et al., 1977; Rabinowitz and LaBrecque, 1977, 1979). Their element patterns are shown in Figure 12. The REE pattern of RJS-36 shows depletion in light REE, indicating it is very similar to MORBs. The low K, Sr, Th, and U concentrations suggest it may be oceanic basalt. However, ~25% lower Al, ~20% lower Ti, ~5× lower Cr, and ~33% higher total Fe contents, respectively, in RJS-36 relative to the average composition of MORBs questions the precise classification of RJS-36 as a typical MORB. ESS-9 shows light REE enrichment, indicating it is an alkalic (K_2O = 1.0%) basalt. The compositions of alkalic basalt samples RJS-33, RJS-87, and SPS-4A are intermediate between RJS-36 and ESS-9. They all show moderate light REE enrichment. The significant depletion of Th relative to Ta in basalts ESS-9, RJS-33, RJS-87, and RJS-36 are reminiscent of similar Th/Ta ratios found in Eocene Siletz alkalic basalts in the Oregon Coast Range mountains, in low K_2O (0.1–0.3%) basalts in the Crescent Karmutsen and Metchosin formations in the northwest Washington to Vancouver coast ranges (Hill, 1975), and in Hawaiian tholeiitic basalts (Budahn, 1980). For seven out of the ten different lunar basalts for which both Ta and Th were measured, only the Apollo 17 high TiO_2 mare basalts also exhibit a low chondrite-normalized Th/Ta ratio. Very likely the source matter from which the Th-poor basalts were derived by partial melting was depleted in Th relative to Ta.

RJS-87 is located near the RJS-36 site, but closer to the coast. Although the bulk chemistries of RJS-87 and RJS-36 are quite similar, RJS-87 shows moderate K, Ba, and light REE, Hf, Ta, and Th enrichments, whereas the heavy REE and Sc are the same relative to basalt RJS-36. A smaller degree of partial melting for the

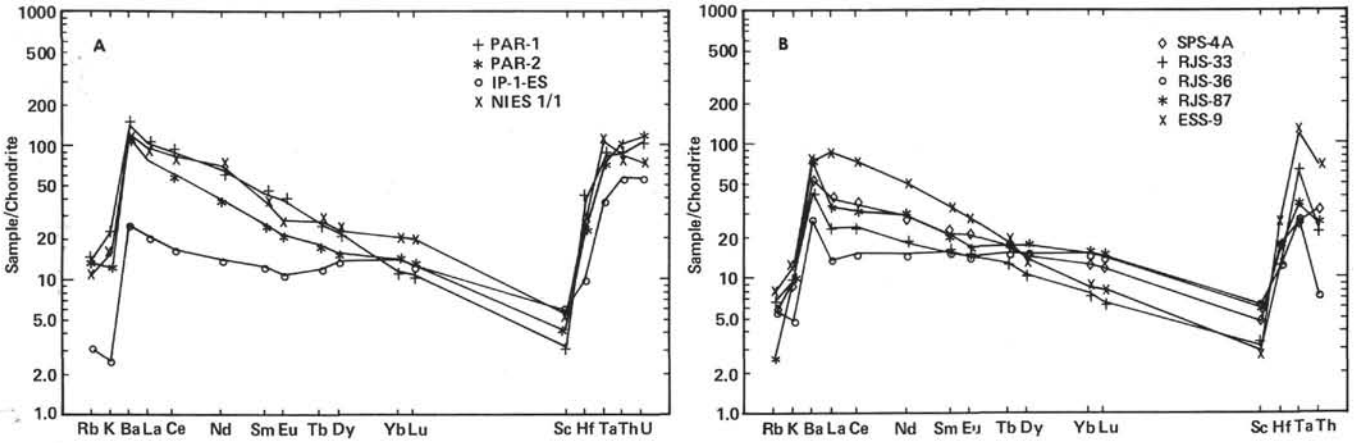

Figure 12. Chondrite-normalized element concentration patterns of basalt samples taken (A) along the Brazil coast, (B) from the continental margin off Brazil. REE and Sc are in units of eight-coordinated ionic radii.

genesis of RJS-87 could be interpreted as the primary factor for the enrichments observed in RJS-87 relative to RJS-36. Their REE patterns are reminiscent of the transition of REE patterns from oceanic basalts depleted in light REE to the volcanics of continental Japan enriched in light REE (Masuda, 1968).

Paraná basalts are between 119 and 147 Ma old, with the maximum of activity about ~125 Ma. During this period, there also were volcanic activities along the Brazilian coast (Amaral et al., 1966; Melfi, 1967; Herz, 1977). On the African side, Siedner and Miller (1968) have determined the age of Kaoko basaltic rocks from Southwest Africa directly opposite their counterparts in Brazil. The ages fall in the interval 114 to 136 Ma, with the maximum at ~125 Ma.

From these age results and the data of our samples on the continental margin, some speculations about the South America–Africa continental drift may be suggested. Basaltic sample SPS-4A has been dated at approximately 138 Ma (E. H. McKee, U.S.G.S. pers. comm.), almost the same age as the oldest Paraná basalt, indicating that volcanic activities also occurred on the South American continental margin at the same period. Also, there is evidence which suggests elevated submarine volcanos were active near the continental margin of Southwest Africa (Hekinian, 1972). It is very likely that volcanism on the continents along the coasts and on the continental margins was associated with the initial separation of South America and Africa.

We have chemically identified sample RJS-36, dated at ~112 Ma by E. H. McKee (U.S.G.S.), as a possible MORB. This early MORB is, to our knowledge, the oldest oceanic tholeiitic basalt recovered from the South Atlantic. We suggest that ~112 Ma South America and Africa were quite close and that a shallow sea separated the continents, similar to the Red Sea Axial Trough spreading center between the African and Arabian continents. With considerable continental pressure above the mantle adjacent to such a shallow trough, it is expected that partial melting of upper mantle matter would yield lower Al and Cr and higher Fe contents in the early-stage MORBs. As spreading increased, the pressure from the continents over the mantle adjacent to the mid-oceanic ridge would decrease, and partial melting might occur at greater depths, thereby yielding higher Al and lower Fe contents in younger MORBs. Moreover, MORB formed during the early stages of a spreading center between two continents would be expected to be presently located on a continental margin; such is the case for the 112 Ma old Sample RJS-36, now on the South American margin.

Young MORBs along the Red Sea Axial Trough have lower Al, Ti, and Cr, and higher Fe contents than MORBs; their REE patterns, however, are similar to the MORBs (Schilling, 1969; Coles, 1973). This evidence from a recent spreading center at the Red Sea supports the conclusion that sample RJS-36 is an early-stage MORB.

A tholeiitic basalt cored from the Brazilian Basin, Site 355, Leg 39, is dated at 78 Ma (McKee and Fodor, 1977). These results suggest that South America and Africa started drifting apart to form the South Atlantic ocean floor $\geq$112 Ma.

CONCLUSIONS

1. The downcore element concentration profiles and regression analyses show that the REE are present in both carbonate and noncarbonate phases. Sr follows Ca, indicating it is in the carbonate phase. Most other elements are present essentially in the noncarbonate phase.

2. The partition coefficients (referred to as free ion concentrations in seawater) of the REE between carbonate and seawater are high and increase with decreasing REE ionic radii from 3.9×10^6 for La to 15×10^6 for Lu. The apparent partition coefficients (referred to as total concentration of an element in seawater) pass through a maximum around Ce and Nd.

3. Calculations indicate that over the past 70 Ma the lanthanide concentrations have not changed very much in the ocean between two drifting continents. The results also imply that the bulk composition of seawater has been quite constant during this period.

4. The relative REE abundance pattern in carbonate from sediment Sample 525A-1-3, 15–17 cm (~0.3 Ma old) resembles the REE pattern in modern seawater, and

both exhibit a marked Ce depletion. This suggests that the Ce depletion in carbonate simply reflects Ce^{+3} depletion in seawater, indicating oxidizing conditions similar to modern seawater. The REE pattern in the carbonate phase is a redox indicator of seawater.

5. The REE pattern of mollusk shell segments taken from late Campanian sediments shows no depletion, indicating that the seawater over the Hole 525A area was in a reduction state at that time. Sediment Sample 525A-31-3, 5–6 cm shows a slight Ce depletion, indicating that during the late Paleocene seawater over the Walvis Ridge became more oxidizing. There is a significant change in the Ce anomaly between Samples 525A-31-3, 5–6 cm and 525A-30-4, 50–51 cm (both containing >96% carbonate), indicating that from this period (~54 Ma) on, the oxidizing conditions of seawater over Hole 525A became similar to those in the present ocean. Changes in these conditions were undoubtedly related to continental drift and Walvis Ridge subsidence. As continental drift progressed, the South Atlantic opened wider, the Walvis Ridge subsided deeper, the water passage between northeast Brazil and west central Africa became wider, and the water circulation of the South Atlantic (especially in the Angola Basin) improved. All of these somewhat interdependent secular events resulted in seawater conditions at ~54 Ma that are similar to those of present-day ocean water.

6. Based on our analyses, the compositions of the basement basaltic rocks in Hole 525A are alkalic in nature, not ocean tholeiitic basalt. The results of our REE work support the hypothesis that the Walvis Ridge was formed by a series of volcanos originating from a "hot spot" near the Mid-Atlantic Ridge, and that these volcanos were subsequently transported eastward as seafloor spreading progressed during continental drift.

ACKNOWLEDGMENTS

This work was financially supported by the Radiation Center, O.S.U., Dr. C. H. Wang, Director, and by the Ministry of Education and the Institute of Atomic Energy, Beijing, China. We wish to thank the following reviewers for their critical perusal of this manuscript: Drs. E. J. Dasch, J. Dymond, R. V. Fodor and D. Z. Piper. We also acknowledge the assistance of T. V. Anderson, W. T. Carpenter, Dr. M.-S. Ma, M. R. Smith, and V. N. Smith for help in various aspects of the neutron activations, data reduction and discussions.

REFERENCES

Amaral, G., Cordani, U. G., Kawashita, K., and Reynolds, J. H., 1966. Potassium-argon dates of basaltic rocks from southern Brazil. *Geochim. Cosmochim. Acta*, 30:159–189.

Baker, P. E., Gass, I. G., Harris, P. G., and LeMaitre, R. W., 1964. The volcanological report of the Royal Society Expedition to Tristan da Cunha, 1962. *Phil. Trans. R. Soc. London, Ser. A.*, 256: 439–576.

Bender, M., Broecker, W., Gornitz, V., Middel, U., Kay, R., Sun, S.-S., and Biscaye, P., 1971. Geochemistry of three cores from the East Pacific Rise. *Earth. Planet. Sci. Lett.*, 12:425–433.

Bolli, H. M., Ryan, W. B. F., and Shipboard Scientific Party, 1978a. Angola continental margin—Sites 364 and 365. *In* Bolli, H. M., Ryan, W. B. F., et al., *Init. Repts. DSDP*, 40: Washington (U.S. Govt. Printing Office), 357–390.

_____, 1978b. Walvis Ridge—Sites 362 and 363. *In* Bolli, H. M., Ryan, W. B. F., et al., *Init. Repts. DSDP*, 40: Washington (U.S. Govt. Printing Office), 183–236.

Budahn, J. R., 1980. Geochemical study of Hawaiian basalts [M.S. thesis]. Oregon State University.

Carpenter, R., and Beasley, T. M., 1981. Plutonium and americium interaction in anoxic sediments: Evidence against remobilization. *Geochim. Cosmochim. Acta.*

Coles, D. G., 1973. Chemical compositional studies of marginal rift and plateau basalts from Saudi Arabia [M.S. thesis]. Oregon State University.

DePaolo, D. J., and Wasserburg, G. J., 1979. Neodymium isotopes in flood basalts from the Siberian Platform and inferences about their mantle sources. *Proc. Nat. Acad. Sci. USA*, 76:3056–3060.

Elderfield, H., and Greaves, M. J., 1981. Negative cerium anomalies in the rare earth element patterns of oceanic ferromanganese nodules. *Earth Planet. Sci. Lett.*, 55:163–170.

Engel, A. E. J., and Engel, C. G., 1964. Composition of basalts from the Mid-Atlantic Ridge. *Science*, 144:1330–1333.

Engel, A. E. J., Engel, C. G., and Havens, R. G., 1965. Chemical characteristics of oceanic basalts and the upper mantle. *Geol. Soc. Am. Bull.*, 76:719–734.

Erlich, A. M., 1968. Rare-earth abundances in nodules [Ph.D. dissert.]. Massachusetts Institute of Technology, Cambridge, Mass.

Fodor, R. V., Husler, J. W., and Kumar, N., 1977. Petrology of volcanic rocks from an aseismic rise: Implications for the origin of the Rio Grande Rise, South Atlantic Ocean. *Earth Planet. Sci. Lett.*, 35:225–233.

Fodor, R. V., Keil, K., Husler, J. W., and McKee, E. H., 1977. Petrology and K-Ar age of volcanic tuff and ash from the Walvis seamount province, DSDP site 359, Leg 39. *In* Supko, P. R., Perch-Nielsen, K., et al., *Init. Repts. DSDP*, 39: Washington (U.S. Govt. Printing Office), 525–536.

Fodor, R. V., and Thiede, J., 1977. Volcanic breccia from DSDP Site 357: Implications for the composition and origin of the Rio Grande Rise. *In* Supko, P. R., Perch-Nielsen, K., et al., *Init. Repts. DSDP*, 39: Washington (U.S. Govt. Printing Office), 537–543.

Goldberg, E. D., 1961. Chemistry in the oceans. *Oceanography:* (Am. Ass. Advanc. Sci.), pp. 582–597.

Goldberg, E. D., Koide, M., Schmitt, R. A., and Smith, R. H., 1963. Rare earth distribution in the marine environment. *J. Geophys. Res.*, 68:4209–4217.

Grim, R. E., 1968. *Clay Mineralogy* (2nd ed.): New York (McGraw-Hill).

Hamaguchi, H., Kuroda, R., and Watanabe, Y., 1963. Chemical investigations of deep sea sediments 29. Tantalum content of deep sea sediments. *J. Chem. Soc. Japan*, 84:723–725.

Handbook of Geochemistry (Vol. II-3), 1978: Berlin (Springer-Verlag).

Haskin, L. A., Frey, F. A., Schmitt, R. A., and Smith, R. H., 1966. Meteoritic, solar and terrestrial rare-earth distributions. *Phys. Chem. Earth*, 7:167–321.

Haskin, L. A., and Paster, T. P., 1979. Geochemistry and mineralogy of the rare earths. *In* Gschneider, K. A., Jr., and Eyring, L. (Eds.), *Handbook on Physics and Chemistry of Rare Earths:* Amsterdam (North-Holland Publishing Company), Ch. 21.

Hekinian, R., 1972. Volcanics from the Walvis Ridge. *Nature Phys. Sci.*, 239:91–93.

Herz, N., 1977. Timing of spreading in the South Atlantic: Information from Brazilian alkalic rocks. *Geol. Soc. Am. Bull.*, 88: 101–112.

Hill, D. W., 1975. Chemical composition studies of Oregon and Washington coastal basalts [M.S. thesis]. Oregon State University.

Høgdahl, O. T., Melsom, S., and Bowen, V. T., 1968. Neutron activation analysis of lanthanide elements in sea water. *Adv. Chem. Ser.*, 33:308–325.

Kowsmann, R., Leyden, R., and Francisconi, O., 1977. Marine seismic investigations, south Brazil margin. *Am. Assoc. Pet. Geol. Bull.*, 61:546–557.

Kyte, F. T., Zhou, Z., and Wasson, J. T., 1980. Siderophile-enriched sediments from the Cretaceous/Tertiary boundary. *Nature*, 288: 651–656.

Larson, R. L., and Ladd, J. W., 1973. Evidence for the opening of the South Atlantic in the Early Cretaceous. *Nature*, 246:209–212.

Laul, J. C., 1979. Neutron activation analysis of geological materials, *Atomic Energy Rev.*, 17:603–695.

LeMaitre, R. W., 1962. Petrology of volcanic rocks, Gough Island, South Atlantic. *Geol. Soc. Am. Bull.*, 37:1309–1340.

Liu, Y. G., 1982. Chemical element profiles by instrumental neutron activation analysis in: 1. Two species of wheat bunt spores, *Tilletia*

caries (D.C.) Tul. and *Tilletia controversa* Kuhn; and 2. Representative sediment and basalt samples taken from a DSDP 678-m core, Site 525A, Leg 74, Walvis Ridge [M.S. Thesis]. Oregon State University.

Ma, M.-S., Laul, J. C., and Schmitt, R. A., 1981. Complementary rare earth element patterns in unique achondrites, such as ALHA 77005 and shergottites, and in the earth. *Proc. 12th Lunar Planet. Sci. Conf.:* New York (Pergamon), pp. 1349–1358.

McKee, E. H., and Fodor, R. V., 1977. K-Ar age of deep-sea basalt, Brazil Basin, Leg 39 Deep Sea Drilling Project. *In* Supko, P. R., Perch-Nielsen, K., et al., *Init. Repts. DSDP*, 39: Washington (U.S. Govt. Printing Office), 545–546.

Masuda, A., 1968. Geochemistry of lathanides in basalts of central Japan. *Earth Planet. Sci. Lett.*, 4:284–292.

Melfi, A., 1967. Potassium-argon ages for core samples of basaltic rocks from southern Brazil. *Geochim. Cosmochim. Acta*, 31: 1079–1089.

Morgan, W. J., 1971. Convection plumes in the lower mantle. *Nature,* 230:42–43.

_____, 1972. Plate motions and deep mantle convection. *Geol. Soc. Am. Mem.*, 132:7–22.

Natland, J. H., 1978. Composition, provenance, and diagenesis of Cretaceous clastic sediments drilled on the Atlantic continental rise off southern Africa, DSDP Site 361—implications for the early circulation of the South Atlantic. *In* Bolli, H. M., Ryan, W. B. F., et al., *Init. Repts. DSDP*, 40: Washington (U.S. Govt. Printing Office), 1025–1061.

Parekh, P. P., Möller, P., Dulski, P., and Bausch, W. M., 1977. Distribution of trace elements between carbonate and non-carbonate phases of limestone. *Earth Planet. Sci. Lett.*, 34:39–50.

Parratt, L. G., 1961. *Probability and Experimental Errors in Science:* New York (John Wiley & Sons), p. 130.

Piper, D. Z., 1974. Rare earth elements in the sedimentary cycle: a summary. *Chem. Geol.*, 14:285–304.

Rabinowitz, P. D., and LaBrecque, J., 1977. The isostatic gravity anomaly: A key to the evolution of the ocean-continent boundary. *Earth Planet. Sci. Lett.*, 35:145–150.

_____, 1979. The Mesozoic South Atlantic Ocean and evolution of its continental margins. *J. Geophys. Res.*, 84:5973–6002.

Reyment, R. A., 1969. Ammonite biostratigraphy, continental drift and oscillatory transgressions. *Nature*, 224:137–140.

Ryan, W. B. F, Bolli, H. M., Foss, G. N., Natland, J. H., Hottman, W. E., and Foresman, J. B., 1978. Objectives, principal results, operations, and explanation notes of Leg 40, South Atlantic. *In* Bolli, H. M., Ryan, W. B. F., et al., *Init. Repts. DSDP*, 40: Washington (U.S. Govt. Printing Office), 5–28.

Schilling, J. G., 1969. Red Sea origin: Rare earth evidence. *Science*, 165:1357–1360.

Shanbhag, P. M., and Morse, J. W., 1982. Americium interaction with calcite and aragonite surface in sea water. *Geochim. Cosmochim. Acta.*, 46:241–246.

Shannon, R. D., 1976. Revised effective ionic radii and systematic studies of interatomic distances in halides and chalcogenides. *Acta Cryst. V. A*, 32:751–767.

Siedner, G., and Miller, J. A., 1968. K-Ar age determinations on basaltic rocks from South-West Africa and their bearing on continental drift. *Earth Planet. Sci. Lett.*, 4:451–458.

Sillen, L. G., Högfeldt, E., Martell, A. E., and Smith, R. M., 1971. *Stability Constants. Supplement No. 1.,* Chem. Soc. London Spec. Publ., 25.

Spirn, R. V., 1965. Rare earth distributions in the marine environment [Ph.D. dissert.]. Massachusetts Institute of Technology, Cambridge, Mass.

Supko, P. R., Perch-Nielsen, K., and Shipboard Scientific Party, 1977a. Site 359: Walvis Ridge (seamount). *In* Supko, P. R., Perch-Nielsen, K., et al., *Init. Repts. DSDP*, 39: Washington (U.S. Govt. Printing Office), 373–392.

_____, 1977b. Site 357: Rio Grande Rise. *In* Supko, P. R., Perch-Nielsen, K., et al., *Init. Repts. DSDP*, 39: Washington (U.S. Govt. Printing Office), 231–328.

_____, 1977c. Site 356: São Paulo Plateau. *In* Supko, P. R., Perch-Nielsen, K., et al., *Init. Repts. DSDP*, 39: Washington (U.S. Govt. Printing Office), 141–230.

Supko, P. R., Perch-Nielsen, K., and Carlson, R. L., 1977. Introduction and explanatory notes, Leg 39, Deep Sea Drilling Project. *In* Supko, P. R., Perch-Nielsen, K., et al., *Init. Repts. DSDP*, 39: Washington (U.S. Govt. Printing Office), 5–24.

Tatsumoto, M., Hedge, C. E., and Engel, A. E. J., 1966. Potassium, rubidium, strontium, thorium, uranium and the ratio of strontium-87 to strontium-86 in oceanic tholeiitic basalt. *Science*, 150: 886–888.

Turekian, K. K., 1968. *Oceans:* Englewood Cliffs, New Jersey (Prentice-Hall, Inc.), p. 92.

Turekian, K. K., Katz, A., and Chan, L., 1973. Trace element trapping in pteropod tests. *Limnol. Oceanogr.*, 18:240–249.

Turekian, K. K., and Wedepohl, K. H., 1961. Distribution of the elements in some major units of the Earth's crust. *Geol. Soc. Am. Bull.*, 72:175–192.

Turner, D. R., Whitfield, M., and Dickson, A. G., 1981. The equilibrium speciation of dissolved components in freshwater and seawater at 25°C and 1 atm pressure. *Geochim. Cosmochim. Acta*, 45: 855–881.

Whittaker, E. J. W., and Muntus, R., 1970. Ionic radii for use in geochemistry. *Geochim. Cosmochim. Acta*, 34:945–956.

Wildeman, T. R., and Haskin, L., 1965. Rare earth elements in ocean sediments. *J. Geophys. Res.*, 70:2905–2910.

Wilson, J. T., 1963. Evidence from islands on the spreading of ocean floors. *Nature*, 197:536–538.

_____, 1965. Submarine fracture zones, aseismic ridges and the International Council of Scientific Unions Line: Proposed Western margin of the East Pacific Ridge. *Nature*, 207:907–911.